KAPITEL 1 / *CHAPTER 1* [1]
CURRENT STATE OF DEVICES FOR MEASURING PHYSICAL QUANTITIES

DOI: 10.30890/2709-2313.2025-41-07-007

Introduction

In recent years Wireless sensor networks (WSNs) and remote sensor systems are used as part of several important industries, such as social services, military, critical infrastructure monitoring, environmental monitoring, and information collection and processing systems. A large number of organizations are striving to manage their business, operations, and administrations in a versatile, dynamic, and learning-oriented style [1-4]. Activities such as distance learning, environmental education, human services, home and military security, etc. require an exceptional framework that can provide constant, secure, reliable, and versatile information with legitimate data or the basis for learning administration in the context of their limited environment [5-7].

The availability of Internet connections and low manufacturing costs have led to a boom in smart objects, devices with a three-way design consisting of a central processing unit, memory, and wireless connectivity. These smart devices are equipped with sensors that measure, process, and transmit data, as well as devices that can receive commands. Such devices have spread across all areas, and their use is expected to grow exponentially in the future. For these devices, central processing of data has proven advantageous due to numerous factors, including the ability to easily retrieve information from vast repositories and efficiently allocate computing resources. Because of these factors, many devices can benefit from processing only some data locally and offloading other information to central servers. Among the aforementioned devices, which are increasingly present in modern life, are robots. Examples such as the iRobot Roomba, a robot, represent affordable automated tools for everyday life. In addition, Amazon and Google are researching and developing platforms for delivering

[1]***Authors:*** *Osadchuk Oleksandr Volodumurovuch, Osadchuk Iaroslav Oleksandrovuch*
Number of characters: *102272*
Author's sheets: *2,56*

consumer products using drones. Most of these robots have limited built-in computing power, but still generate large amounts of data. Cloud-based data analysis of such robots poses many challenges due to the tight latency requirements and the large amount of data received [8].

Currently, radio measuring devices that simultaneously measure and wirelessly transmit informative signals about the state of pressure, humidity, temperature, optical radiation power, magnetic field induction, and gas composition and concentration in the environment are practically absent in world practice.

1.1. Analysis of different types of IoT sensors and networks

The outstanding achievements of micro- and nanoelectronics in the last decade have been mainly implemented in information processing and computing equipment. Electronic communication control systems also require the implementation of achievements of micro- and nanoelectronic circuit technology, primarily for radio-technical devices for measuring physical quantities, as well as for electronic information processing equipment and executive bodies [1-9].

The increasing exploitation of smart environments, audio and video streams is driving the mass adoption of sophisticated IoT systems. Information and measurement equipment and wireless sensor networks are deployed to monitor a variety of phenomena, providing a wealth of heterogeneous measurements and multimedia data. The data is then stored, transmitted and processed for many purposes, such as healthcare, air quality monitoring and security system management. For many years, corporate organizations have accumulated growing stocks of data, conducted analytics on this data to benefit from large volumes of information, and developed applications exclusively for processing this data. However, a new trend is emerging where measurement data acquisition, information management and application development are decoupled, thus giving business companies different roles in the market [10]. In such a scenario, flexible solutions are needed to integrate measurement devices, systems for processing, transmitting and storing measurement information and

providing the final product in the form of real-time final information to the end user. From the perspective of the Internet of Things (IoT), a huge number of physical sensors and devices are interconnected via the Internet to provide a wealth of heterogeneous, complex, and unstructured data. Much effort in the industry and research community has been focused on storing IoT data to balance the cost and performance of data maintenance and analysis. The development of powerful data storage systems can effectively cope with the demands of big data applications, and cloud computing is expected to play a significant role in the IoT paradigm [11]. Cloud storage offers a large number of opportunities for storing and processing informative signals and data at scale [12]. From the perspective of the Cloud user, data collected from the monitoring infrastructure is provided in a single way, which is designed according to the Sensor Web Enablement (SWE) specifications defined by the Open Geospatial Consortium (OGC) [5–8].

One of the leading places in information and measuring technology is occupied by devices for measuring and controlling gas concentration, pressure, humidity, magnetic field induction, optical radiation and temperature [1–4]. The development and improvement of this class of measuring devices are due to the increased requirements for the accuracy and sensitivity of measuring physical quantities by sensors with autonomous decision-making for robotic devices, remote control systems, and specialized cloud platforms [9, 10].

Today, a fairly large number of various devices for measuring and controlling gas concentration, pressure, humidity, magnetic field induction and temperature are known [1–10]. The development of the theory and practical application of sensors in Ukraine is carried out by such scientific institutions as NTUU “Kyiv Polytechnic Institute” (Kyiv), Taras Shevchenko Kyiv National University (Kyiv), “Lviv Polytechnic” National Technical University (Lviv), Institute of Cybernetics of the NAS of Ukraine (Kyiv), Institute of Thermal Physics of the NAS of Ukraine (Kyiv), Institute of Semiconductor Physics of the NAS of Ukraine (Kyiv), Institute of Metrology (Kharkiv), Kharkiv National Technical University (Kharkiv), Odessa National University named after I.I. Mechnikov (Odessa), Vinnytsia National Technical

University (Vinnytsia).

The Internet of Things (IoT) connects everything, both living and non-living, leading to revolutionary changes in society [11]. Infrastructure objects are connected through various network environments. The main goal of IoT is to make things more dynamic and convenient. The IoT domain has significantly increased the number of smart devices, allowing many objects or devices to act as smart things. IoT-enabled objects have been embedded with intelligent capabilities through a variety of tools and technologies, such as sensors, RFID, and many other forms of embedded computing [12]. IoT technology has led people to ubiquitous connectivity and smart services. It is now widely deployed in various intelligent applications and creates a wide range of opportunities for industry, business, and military equipment [13].

IoT consists of various domains, including cloud, mobile devices, virtualized environments, sensors, radio frequency identification (RFID), and artificial intelligence [13]. In addition, various intelligent services are offered in IoT-based networks, which has led to IoT cloud networks [4]. In this intelligent environment, IoT devices can exchange information and provide many convenient services. For example, Alexa-enabled echo devices and many other smart IoT devices provide owners with many capabilities, such as turning on and off indoor and outdoor electronic devices, lights, water heaters, washing machines, air conditioners, and more [5]. Devices such as Echo Spot and Alexa make audio and video calls, play music, watch videos, view news, view calendars, to-do lists, manage traffic, view social media accounts, monitor children, control lights, and more [5]. Sensors play an important role in the automation of any application by measuring and processing the collected data to detect changes in physical processes. Accordingly, when there is a change in any physical state for which the sensor is used, it gives a measurable response. There are different types of sensors, from simple to quite complex. The classification of sensors can be based on their specifications, conversion method, type of material used, physical phenomenon being measured, and area of application [1–6].

Network technologies allow devices to IoT devices communicate with other devices, applications, and services running in the cloud [7]. The Internet relies on

standardized protocols to provide secure and reliable communication between disparate devices. Standard protocols define the rules and formats that devices use to establish and manage networks and transmit data over those networks [7]. Networks are built as a "stack" of technologies. A technology such as Bluetooth LE is at the bottom of the stack [8]. While others, such as IPv6 technologies (which are responsible for logical device addressing and network traffic routing), are further up the stack. Technologies at the top of the stack are used by applications running on top of these layers, such as message queuing technologies.

IoT networking technologies to be aware of at the bottom of the protocol stack include cellular, Wi-Fi, and Ethernet, as well as more specialized solutions such as LPWAN, Bluetooth Low Energy (BLE), ZigBee, NFC, and RFID [14]. According to Gartner, NB-IoT is emerging as the standard for LPWAN networks. The following are the networking technologies with a brief description of each [14]:

LPWAN (Global Low Power Network) is a category of technologies designed for long-range, low-power wireless communication. They are ideal for large-scale deployment of low-power IoT devices such as wireless sensors. LPWAN technologies include LoRa (Long Range Physical Layer Protocol), Haystack, Sig Fox, LTE-M, and NB-IoT (Narrowband IoT) [15].

Honeycomb LPWAN NB-IoT and LTE-M standards address low-power and low-cost IoT communication options using existing cellular networks. NB-IoT is the newest of these standards and is aimed at long-range communication between a large number of devices, mostly indoors. LTE-M and NB-IoT were developed specifically for IoT, but existing cellular technologies are also often used for long-range wireless communication [15]. While this included 2G (GSM) in legacy devices (and is now being phased out), CDMA (also being phased out or discontinued), it also includes 3G, which is rapidly being phased out as several network providers are phasing out all 3G devices. 4G is still active until 5G becomes fully available and deployed.

Bluetooth Low Energy (BLE) is a low-power version of the popular 2.4 GHz Bluetooth wireless protocol. It is designed for short-range communication (up to 100 meters), typically in a star configuration, with a single master device controlling

multiple slave devices [16]. Bluetooth operates at both layers 1 (PHY) and 2 (MAC) of the OSI model. BLE is best suited for devices that transmit small amounts of data in bursts [16]. Devices are designed to sleep and conserve power when they are not transmitting data. Personal IoT devices, such as wearable health and fitness trackers, often use BLE.

ZigBee operates at the 2.4 GHz wireless frequency. It has a longer range than BLE, up to 100 meters. It also has a slightly lower data rate, a maximum of 250 Kbps, compared to 270 Kbps for BLE. ZigBee is a mesh protocol [34]. Unlike BLE, not all devices can sleep between packets. Much depends on their position in the mesh and whether they need to act as routers or controllers in the mesh. ZigBee is designed for building and home automation applications. Another technology closely related to ZigBee is Z-Wave, which is also based on IEEE 802.15.4. Z-Wave was developed for home automation [17].

NFC stands for Near Field Communication (NFC), a protocol used for communication over very short ranges (up to 4 cm), such as when an NFC card or tag is held close to a reader [17]. NFC is often used for payment systems, but is also useful for registration systems and smart tags for asset tracking.

RFID stands for Radio Frequency Identification, and RFID tags store identifiers and data [15]. Tags are attached to devices and are read by an RFID reader. The typical range of RFID is less than a meter. RFID tags can be active, passive, or assistive. Passive tags are ideal for devices without batteries because the identifier is passively read by the reader. Active tags broadcast their identifier periodically, while assistive passive tags become active when an RFID reader is present [15]. This communication protocol, which uses active RFID, is designed for use in Industrial IoT applications for secure long-range communication [17]. Similar to NFC, a typical use case for RFID is inventory tracking in retail and industrial IoT applications.

Wi-Fi is a standard wireless network based on the IEEE 802.11a/b/g/n specifications. 802.11n offers the highest data throughput, but at the cost of high power consumption, so IoT devices may only use 802.11b or g for power conservation reasons [18]. Although Wi-Fi is used in many prototypes and the current generation of IoT

devices, as longer-range, lower-power solutions become more widely available, it is likely that Wi-Fi will be replaced by lower-power alternatives [18].

Ethernet is widely deployed for wired connectivity in local area networks, implementing the IEEE 802.3 standard [19]. Not all IoT devices are or need to be wireless. For example, sensors installed in a building automation system may use wired networking technologies such as Ethernet. Powerline communication, an alternative wired solution, uses the existing electrical network instead of dedicated network cables [19]. Fig. 1 presents the different types of sensors in IoT, which are briefly explained below.

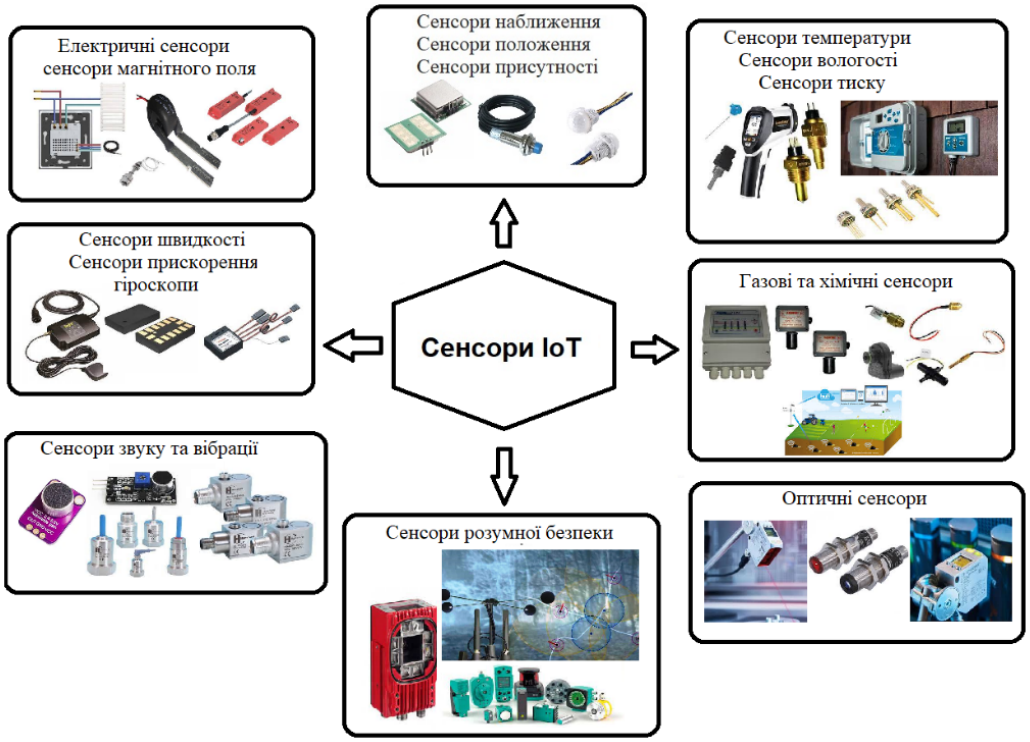

Figure 1 – Different types of IoT sensors

Proximity sensors. The position of any nearby object can be easily determined by a proximity sensor without physical contact. By emitting electromagnetic radiation such as infrared, it detects the presence of the object by simply looking for any variation in the return signal [19]. There are different types of proximity sensors such as inductive, capacitive, ultrasonic, photoelectric, magnetic, etc., designed for different applications. This particular type of sensor is mainly used in applications that require safety and efficiency. The various applications of this type of sensor are object

detection, object counting, rotation measurement, object positioning, material detection, direction measurement, parking sensors, etc. Proximity sensors have wide applications in many industries [20].

Position sensors. A position sensor detects the presence of a person or objects in a certain area by sensing their movement [21]. It can be used in a home security system to allow the owner to monitor the doors and windows of rooms and appliances from anywhere. This allows them to know the open or closed status at any time and can track intruders in their absence. It can be used in healthcare monitoring, to monitor the position of patients, medical staff and doctors in medical facilities, and in agriculture to determine the position of livestock.

Presence sensors. A presence sensor detects the presence of people or objects in a certain area. It can be used for remote monitoring of various parameters, such as temperature, humidity, light, and air quality. A similar application of this type of sensor is given by the authors in [22].

Motion sensors. The motion detector is a device used to detect all kinetic and physical movements in the environment. An application for monitoring homes when the homeowner is away can use motion sensors, and whenever motion is detected, photos or videos can be uploaded to a server. The authors in [23] used a motion detection sensor for home security.

Speed sensors. It is a sensor that calculates the rate of change of a constant position measurement and position value at known intervals. A speed sensor can be linear or angular. A linear speed sensor determines the speed of an object along a straight line, while an angular speed sensor determines the rotational speed of the device. It can be used in smart city applications for intelligent vehicle monitoring [23].

Temperature sensors. Temperature sensors help detect physical changes in one's body by measuring thermal energy. The authors in [24] used temperature sensors to monitor environmental environmental conditions. The collected data is then sent to the cloud via Wi-Fi for analysis. All this is done using an Android smartphone. A similar type of sensor is also used by the authors in [24] for smart agriculture and allows farmers to increase overall yield and product quality by receiving real-time data about

their land.

Pressure sensors. Pressure sensors detect the magnitude of force and convert it into signals. This type of sensor can be used in health monitoring [25].

Chemical and gas sensors. A gas or chemical sensor is an analytical device used to measure the chemical composition of an environment. Air quality monitoring can be performed using a wireless network of gas and chemical sensors by monitoring chemical plumes in the environment.

Humidity sensors. The humidity sensor measures air temperature as well as humidity and signals the humidity of the environment. The authors in [26] used humidity sensors for smart agriculture, which allowed farmers to increase the overall yield and quality of products by receiving data about their land in real time. A similar application is also proposed in [26], where the collected data is senton the open source platform thing speak.

Water quality sensors. Water quality sensors are used to monitor ions. Water quality is measured by water quality sensors. Researchers in [27] presented a design for a low-cost measurement system temperature, PH, turbidity, electrical conductivity, dissolved substrate water with control water quality in the IoT system.

Infrared sensors. Infrared sensors emit or detect infrared radiation to sense some characteristics of certain objects. They can also measure heat emission. This type of sensor can be used for home automation, monitoring and controlling household appliances, such as turning lights on and off [28]. It can also be used for smart security, waste collection systems, smart parking.

Gyroscope sensors. Gyroscope sensors detect any tilt or angular movement of an object by measuring angular velocity. It is widely used in 3D mouse games, for athlete training, robotics, industrial automation, and many more.

Optical sensors. Optical sensors are useful for detecting electromagnetic energies such as light. Being passive to all forms of electrical interfaces, they are widely used in IoT applications such as digital cameras. Optical sensors are suitable for IoT applications related to energy, healthcare, environment, oil refineries, chemical industry, aerospace industry, etc.

1.2. Temperature sensors with frequency output signal

Different types of sensors have their own advantages and disadvantages, and the most suitable temperature sensor should be selected according to different applications. Depending on the temperature measurement device, semiconductor temperature sensors can be divided into CMOS, bipolar type, resistive type, full MDM transistor type, and thermal dissipation (TD) type [29]. Based on the current basic architecture, integrated CMOS temperature sensors on the chip can be divided into two categories: voltage-domain temperature sensors and time-domain temperature sensors [29]. That is, voltage-domain temperature sensors convert temperature into a corresponding voltage value by means of their temperature sensor module, and an analog-to-digital converter (ADC) is usually used to convert the voltage signal into a digital signal to convert from temperature to digital output [30]. The specific choice of ADC type usually depends on the temperature sensor module and the system indicators. Time-domain temperature sensors convert the voltage or current signal generated by the temperature sensor module into the time domain for processing, such as temperature-related frequency, period, or duty cycle, to output digital encoding. Different architectures lead to differences in the selection of analog-to-digital conversion circuits, which directly affects the performance differences of temperature sensors. CMOS voltage-domain temperature sensors often face problems such as complex structure, large area, and high power consumption due to the selection of ADCs. However, their accuracy is generally high. On the other hand, there are time-domain temperature sensors because they choose digital circuits such as time-to-digital converter (TDC) or frequency-to-digital converter (FDC). A large number of circuit solutions can be created based on them using standard cell libraries, so they have high adaptability, simple structure, small area, and low power consumption.

In [31], an embedded temperature sensor with temperature-to-frequency conversion mode is presented, which can reduce the influence of some variable interferences such as power supply voltage, device and process deviation to a certain extent by using a dual circuit. The temperature sensor can achieve a temperature

measurement range of 0–100 ◦C, and after two-point calibration, the error is +0.65 ◦C - 0.49 ◦C, the resolution is 0.003 ◦C, the area is 0.059 mm^2, and the power consumption is 32.9 μW. Fig. 2 [31] shows a block diagram of an on-chip temperature sensor. The temperature sensor consists of a current generation circuit proportional to the absolute temperature, a relaxation oscillator with an oscillation frequency proportional to the temperature (OSC-PTAT), a relaxation oscillator with an oscillation frequency independent of the temperature (OSC-CON), and a frequency-to-digital converter circuit. The PTAT current is generated by the temperature sensor circuit and is used to charge the OSC-CON and OSC-PTAT modules.

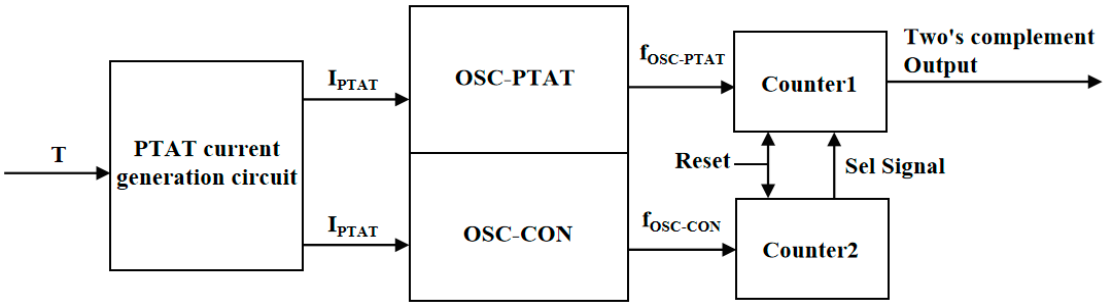

Figure 2 – Block diagram of the temperature measurement principle of the temperature sensor [31]

The OSC-CON module generates a reference clock pulse regardless of temperature, and the OSC-PTAT module generates a clock signal with a frequency proportional to temperature. The two digital converters count the signals generated by the two modules respectively. Both frequency-to-digital converters are controlled by a trigger signal to count simultaneously. When the digital converter of the OSC-CON module reaches its maximum value, it stops counting and triggers the digital converter of the OSC-PTAT module to also stop counting.

The temperature sensor circuit transmits the temperature by following the junction voltage characteristic of the bipolar transistor with the change of temperature. The use of the bipolar transistor as a temperature sensor module has the advantages of high accuracy and high resolution. As shown in Fig. 3, the PNP transistors Q0 and Q1 are connected as diodes, because the number of parallel transistors in the two PNP transistors is different, the voltage on Q0 is VD, the voltage on Q1 is VD1, and the

voltage on the resistor R0 is the voltage difference of the two PNP transistors, ΔV_{BE} [31].

Common oscillation methods include crystal oscillators, traditional RC oscillators, traditional oscillators that use PTAT current to charge and discharge capacitors for oscillation, bandgap ring oscillators, bandgap relaxation reference oscillators, and hybrid oscillators with peak-hold feedback of both relaxation and ring types.

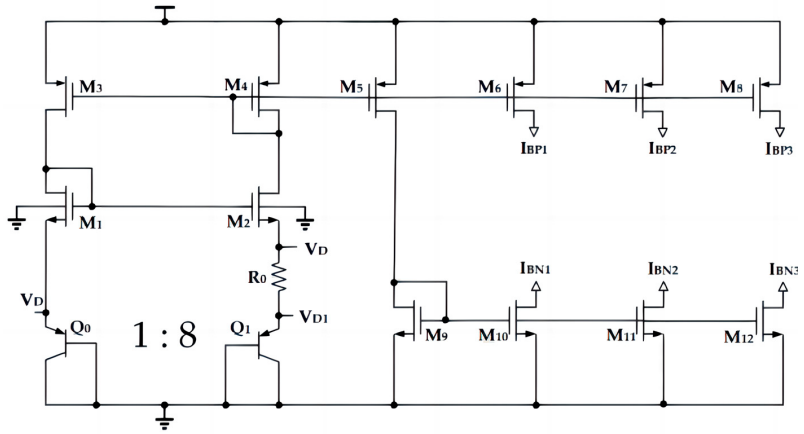

Figure 3 – Current circuit of the temperature sensor [31]

However, all of the above oscillation methods have certain disadvantages. The frequency variation of the waveforms generated by crystal oscillators is about parts per million, but they are expensive and cannot be integrated into a microcircuit. The oscillation frequency variations caused by the circuit structure of traditional RC oscillators, traditional oscillators that use PTAT current to charge and discharge capacitors for oscillation, ring oscillators with bandgap reference, relaxation oscillators with bandgap reference, and hybrid oscillators with peak-holding feedback, both relaxation and ring types, exceed 1% with voltage and temperature changes.

In traditional oscillator circuits that use PTAT current to charge and discharge capacitors to achieve oscillation, variations in the delay td of comparators and RS flip-flops cause frequency variations with voltage and temperature. Aging current sources can degrade the accuracy of the V_{osc} slope and cause frequency variations. The flicker noise of current sources accumulates jitter.

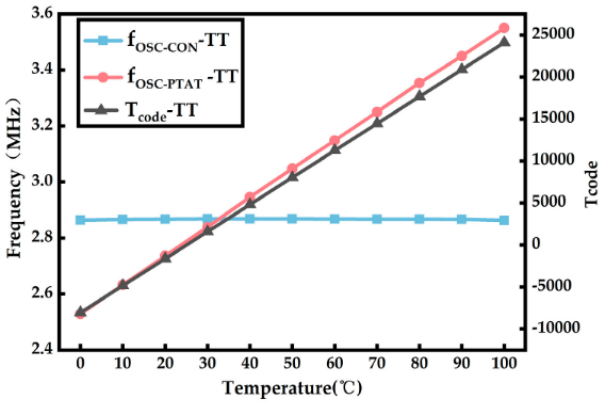

Figure 4 – Dependence of the generation frequency on the temperature change

In [32], the concept of voltage average feedback (VAF) is introduced and an oscillator structure with VAF is proposed, which realizes oscillations by charging and discharging capacitors with PTAT current, as shown in Fig. 5, with the output voltage of the VAF circuit adjusted based on the delay time td of the comparators and RS-flip-flops, thus achieving oscillator stability regardless of the comparator and RS-flip-flop delays, and eliminating the cumulative jitter in the circuit. When the temperature changes from 0 to 100 ◦C, the output frequency of the oscillator changes by 0.08%, thereby improving the frequency stability of the relaxation oscillator.

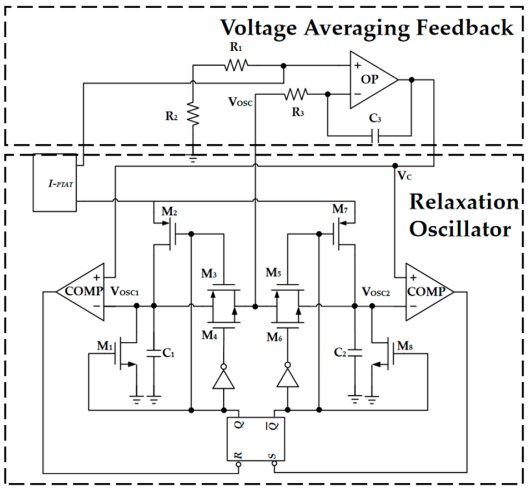

Figure 5 – Schematic diagram of a relaxation oscillator with an oscillation frequency proportional to temperature [32]

Temperature is typically measured using either contact or non-contact methods. Contact approaches are generally more reliable but may require longer measurement

times. Non-contact approaches provide faster temperature measurements at the expense of lower reliability due to the transmittance of the interface medium and the distance of the sensor from the measurement object.

However, when continuous temperature measurements are required, such as measuring human body temperature (at home or in a hospital), lightweight, inconspicuous, and usually battery-free contact sensors are required. To achieve this goal, the use of flexible, wearable sensors is gradually becoming an effective approach for monitoring human body temperature [33]. Near-field communication (NFC)-based temperature sensors have been successfully used in biomedical devices without the use of an electric battery or accumulator [33]. These sensors use embedded active electronic integrated circuits, typically a microcontroller with one or more connected sensors, which must be powered by a reader to transmit the information obtained via a digital communication protocol.

In [34], an alternative solution based on passive resonant sensors was demonstrated, which can be suitably used with flexible portable sensors. A typical disadvantage of flexible sensors is the possible dependence of their characteristics on the bending of the substrate containing the sensing element, which requires appropriate methods to eliminate or reduce this undesirable effect.

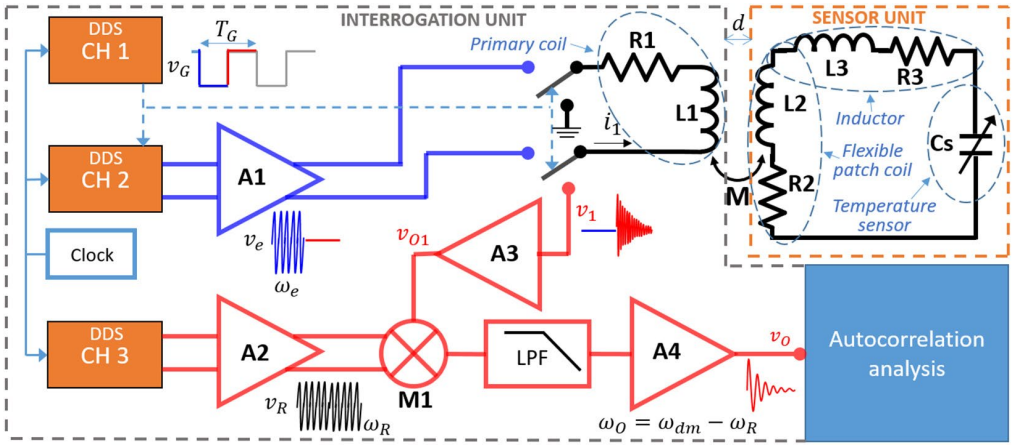

Figure 6 – Block diagram of the contactless survey system [34]

In particular, passive resonant sensors and electromagnetic interrogation methods have been successfully implemented for quartz crystal resonators (QCR), resonant piezolayer (RPL) sensors, MEMS resonators, and LC resonant sensors. For

non-contact interrogation of sensors of this type, both frequency-domain and time-domain approaches can be used. Frequency-domain methods measure impedance, reflection coefficients, or a certain transfer function by simultaneously exciting and sensing the resonator.

In contrast, time-domain methods, as proposed in [34], exploit the transient free response of the resonator, separating the excitation and detection phases in time. The solution proposed in this work uses a non-contact interrogation technique based on magnetic coupling between a passive sensor unit (SU) and an electronic interrogation unit (IU). The SU is based on an RLC resonant circuit and includes a flexible overlay with an inductive copper coil for magnetic coupling, a ceramic capacitor as a temperature-sensitive element, and an additional inductor to make the resonant frequency of the SU independent of the inevitable bending (Fig. 6). The IU contains a primary coil with front-end electronics for non-contact excitation and readout. The proposed approach to interrogating a passive SU offers high accuracy and, at the same time, opens the way to the fabrication of a fully integrated compact system [34].

1.3. Optical sensors

Optoelectronic sensors are widely used in various applications such as medical, automotive, environmental, biochemical, etc. [35]. Many of them are built on integrated light-to-frequency converters that convert light intensity into a quasi-digital (frequency or time signal) in a format for direct connection to a microcontroller, DSP or PC interface [35]. Compared with analog output (voltage or current), the frequency signal as an informative sensor output parameter has a number of advantages, namely: high noise immunity, high reference accuracy, wide dynamic range, multi-parameter, ease of coding, multiplexing, interface and integration [35].

Modern light-to-frequency converters [36] have a wide range of operating frequencies: from tens of Hz to several MHz (Table 1). Although simple frequency-to-digital conversion (based on classical frequency measurement methods) can be performed by any inexpensive microcontroller, the wide dynamic frequency range of

such converters brings, as usual, many design challenges. To obtain acceptable or high metrological characteristics of the developed optical sensor information and measurement systems, frequency-to-digital conversion should be based on advanced frequency measurement methods [36]. Such methods should have a constant relative quantization error over a wide frequency range, scalable resolution, time without redundant conversion, and the ability to measure frequencies exceeding the reference frequency in order to develop sensor systems with reasonable power consumption.

Existing digital light sensors with built-in ADCs on the modern sensor market usually have a sensor Intersil light sensor (ISL29015) which has an integration time of 45-90 ms, and Maxim MAX9635 ADC has a conversion time of 97-107 ms. Such optical sensors with frequency output can be used for proximity or ambient light sensor measurement systems, but they cannot be used for light sensors where conversion speed is a critical parameter. One approach to implementing the above solution is toproblems, the authors in [36] proposed and investigated solutions for frequency optical sensors for various sensor systems, which can be implemented in different technologies: hybrid, standard CMOS technology, System-on-Chip (SoC) and System-in-Package (SiP).The proposed solution is based on the USTI integrated circuit developed by the author [36].

Table 1 – Optical sensors with frequency output [36]

sensor	Characteristics		
	Output frequency. Range	Spectral response, nm	Nonlinear FS error, %
TAOS (USA)			
TSL230	0.4 Hz … 1.1 MHz	350…1000	0.2
TSL235	0.4 Hz … 500 kHz	350…1000	0.2
TSL237	2 Hz … 600 kHz	350…1000	1
TSL245	0.4 Hz … 500 kHz	850…1000	0.2
Hamamatsu(Japan)			
S9705	0 Hz … 1 MHz	300…1000	3
Melexis (Belgium)			
MLX75304	1 Hz … 1.6 MHz	500…1000	No data

This integrated circuit has an extended frequency range up to 9 MHz without pre-scaling and 144 MHz with pre-scaling, reduced relative error to ±0.0005%, increased functionality and reduced conversion time. In [36], a modified dependent reference method for fast and accurate measurement of the frequency and period of electrical signals is proposed, which is used in the USTI integrated circuit (see Fig. 7).

This 2-channel IC has three popular serial interfaces: RS232, I2C and SPI, which are widely used in various sensor systems. It contains three main blocks: a measurement block, a communication block and a time-to-digital converter (TDC). The measurement block provides 2-channel measurements of various time-frequency parameters of electrical signals with a programmable relative error from 1% to 0.0005%: frequency, period, duty cycle, phase shift, time intervals, duty cycle ratio, number of pulses, frequency (period) deviation, ratio and difference of frequencies or periods [37]. The communication block supports three popular serial interfaces, such as RS232, SPI and I2C. TDC is used in a parametric-to-digital converter to directly couple capacitive, resistive and bridge sensing elements to the USTI. The S9705 is a CMOS photointegrated chip that combines a current-to-frequency converter and a photodiode and outputs an oscillation frequency (50% duty cycle) proportional to the intensity of the incoming light incident on the photodiode [37].

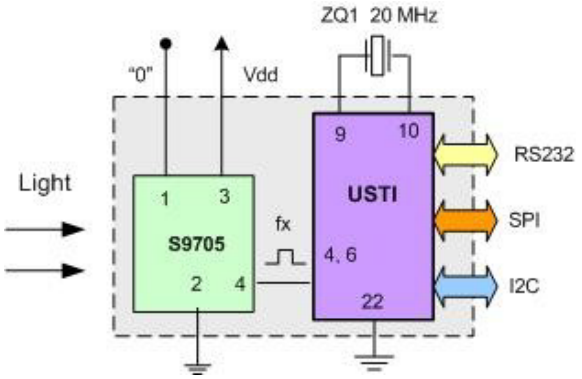

Figure 7 – Schematic diagram of an optoelectronic sensor system based on USTI [36]

Other optical sensors, such as the TCS230 color sensor from TAOS (USA) [37] or the reflective color sensor. The OPB780 from OPTEK Technology can also be

connected in the same way. Intelligent sensors, also known as smart sensors, are usually manufactured using silicon technology in the form of integrated circuits, representing the transducer and electronic circuits together on a single silicon crystal. Thanks to the built-in signal processing functions, such sensors can be connected directly to a microprocessor. This approach minimizes the number of additional electronic components, reduces the cost of the processing system and increases reliability. Successful implementations of this type of sensor for optical and mechanical sensing are well known [36-38], as well as commercial sensors with built-in signal processing, for example, the KPDC0028EA optical sensor from Hamamatsu Photonics Inc. with optical radiation to frequency conversion can be mentioned.

In [38] it is shown that the conversion of light into frequency can be obtained using bipolar sensors developed by integrating micro-sized Schottky diodes (SD) surrounded by metal-oxide-semiconductor (MOS) capacitors into a single crystal. In [38], a bipolar optical sensor was proposed, which presents a digital output in the form of an electrical signal with pulse-width modulation (PWM). To obtain such a digital output, analog-to-digital converters (ADCs) did not need to be built into the sensor chip. When a functional bias voltage is applied to the sensor, the interrelation of the processes of transporting two subsystems of carriers inside the device, namely electrons and holes, leads to the conversion of the input optical signal to a digital electrical signal at the output (Fig. 8). This approach is well suited for the development of inexpensive sensors of a digital output signal. In addition, the sensors proposed in [38], due to their “intelligence”, allow performing logical operations without the need for any additional electronic components. The structure contains a microscopic pin diode surrounded by an MDN capacitor. A microscopic pin diode was fabricated on a high-resistance n-type silicon substrate by diffusing boron through a small window opened in the silicon dioxide layer.

The dependence of the output signal magnitude on the incident optical power is shown in Fig. 9.

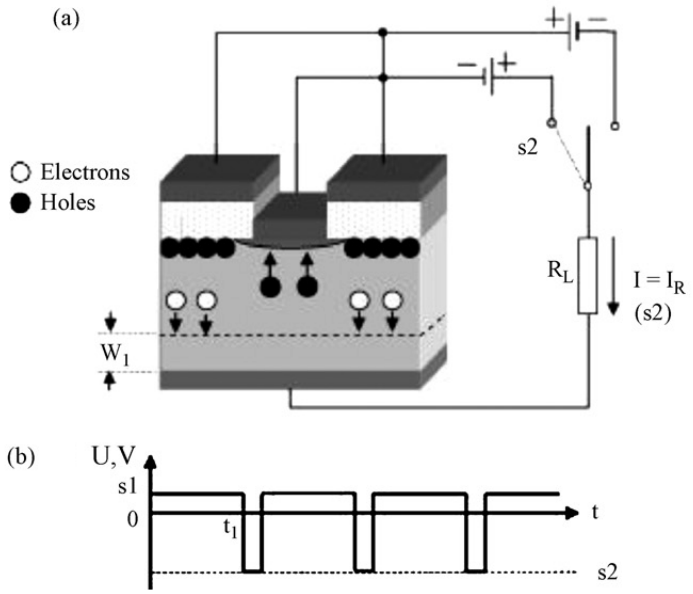

Figure 8 – Cross-section of a simplified sensor structure formed by a microscopic pin diode surrounded by a MDN capacitor [38]

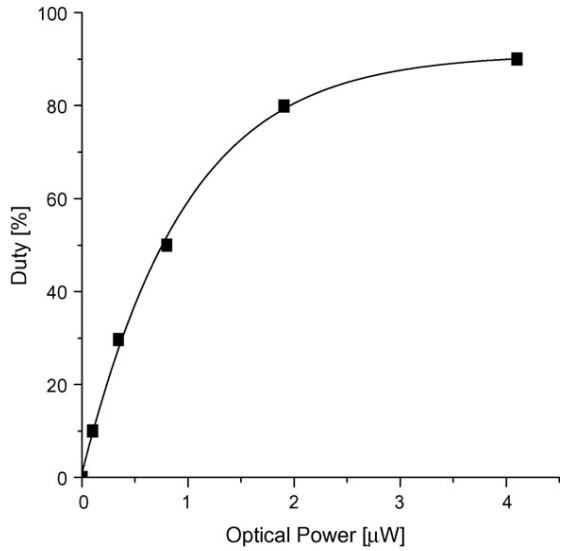

Figure 9 – Dependence of load on incident optical force [38]

Figure 10 shows the PMW output signal from the sensor in dark mode and under illumination with LEDs synchronized on the leading (LED1) and trailing (LED2) edges of negative voltage pulses applied to the ITO electrode [38]. The negative pulse repetition rate is 800 Hz and the load resistor is 1 kΩ.

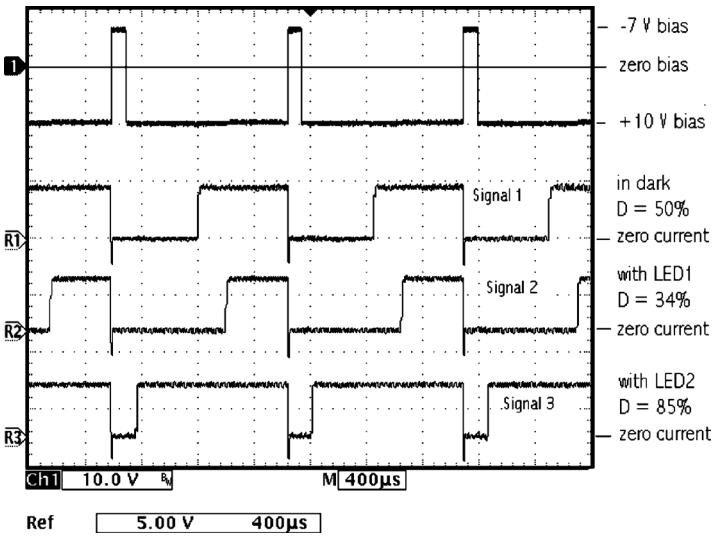

Figure 10 – PWM output signal from an optical sensor [38]

The demand for high-speed wired and wireless communication is constantly increasing, and it is expected that data rates of the order of tens of Gbit/s will be desired in the near future. For the use of higher frequencies such as the millimeter-wave and terahertz frequency ranges, there has been a problem. There are no practical sources and receivers in these ranges, but there are now a number of devices capable of generating high-frequency carriers suitable for communications in the terahertz ranges. One example is resonant tunneling diodes (RTDs), which have the advantage of being potentially very low. RTDs have been the subject of research for many years, leading to useful output power and oscillation frequencies of up to 1.9 THz [39]. Resonant tunneling diodes are compact structures, less than a square millimeter in area, implemented using monolithic microwave integrated circuit (MMIC) technology and have been demonstrated in systems using electrical data modulation up to 34 Gbit/s with a carrier frequency of approximately 500 GHz [39]. Resonant tunneling diodes can be integrated with antennas and other optoelectronic components such as photodiodes. Resonant tunneling diode photodetectors (RTD-PD) have a number of potential applications, such as continuous optical data transmission on a radio frequency carrier and in a fiber optic network as a means for optical synchronization of the generated radio frequency carrier using injection locking [39].

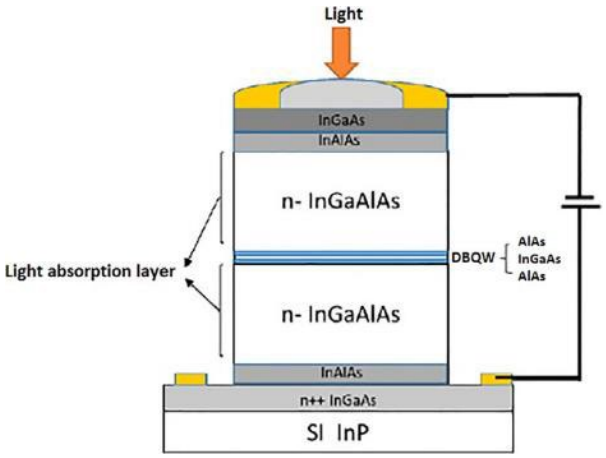

Figure 11 – Structure of the RTD-PD epilayer [39]

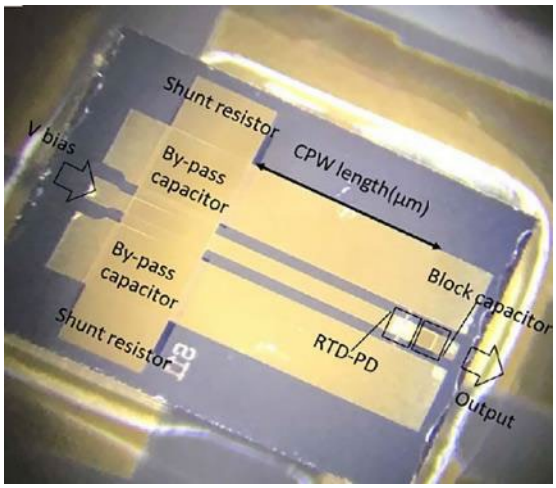

Figure 12 – Photo of the RTD-PD generator with an oscillation frequency of 35 GHz

Figure 11 shows the epilayer structure of the RTD-PD, and Figure 12 shows a microscopic image of the device [39]. These RTD-PDs have an optical window that allows direct access of the optical signal to the generator. As can be seen from the structure, they also include light absorption layers on both sides of the double barrier quantum well (DBQW), which increases the sensitivity to light.

High-speed optoelectronic radio interfaces are a key technology for high-bandwidth wireless communications. Higher data rates require a simultaneous increase in the carrier frequency, leading to systems with data rates in the tens of Gbit/s using carrier frequencies in the hundreds of gigahertz (GHz) [39]. While synthesized multiplier-based systems can be used at high frequencies, the many multiplication

stages result in high power consumption and increased size. An alternative approach is to use oscillators directly at the carrier frequency or to use optical methods to generate the required carrier.

The authors [40] proposed an RTD-based oscillator that can modulate data using electrical or optical signals at a carrier frequency of 79 GHz. The RTD is currently the fastest solid-state electronic device with the highest RTD oscillator frequency of 1.98 THz [40]. RTD-based technologies have several advantages, including their simple circuit design and the ability to generate high-frequency signals with low power consumption. The integration of a double-barrier quantum well (DBQW) with photodetectors by embedding the DBQW in or near the photosensitive region gives rise to a new device known as the RTD-PD. RTD-PDs are considered potential candidates for low-cost integration of radio and fiber networks.

One of the most important features of RTD is the N-shaped I-V characteristic due to the resonant tunneling effect, exhibiting a voltage-controlled negative differential resistance (NDR) region that provides electrical amplification. Due to the nonlinear electrical and optoelectronic properties due to the DBQW structure, RTD-PD exhibits improved photodetection sensitivity, sensitivity, detection dynamic range, and bandwidth efficiency values. Optoelectronic applications of resonant tunneling structures for light detection were proposed in [40]. Thus, it suggests the application of simple high-frequency electrical oscillators and other optoelectronic devices with RTD-PDs that can operate in two modes: non-oscillating (steady-state) or oscillating modes, depending on the operating point. When biased in the positive differential conductance (PDC) region of the IV curve, the RTD-PD exhibits functionality similar to a conventional photodetector, which can absorb an intensity-modulated optical signal and convert it into an electrical signal. When the RTD-PD is biased in the NDC region, it operates in an oscillatory mode, resulting in electrical amplification and high-frequency self-sustained oscillations. The optical modulation characteristics of such an RTD-PD operating in this mode are described in [40].

In [40], an epitaxial layer of RTD-PD was grown on SI-InP containing an undoped indium gallium arsenide (InGaAs) layer (5.7 nm) sandwiched between two undoped

aluminum arsenide (AlAs) barrier layers (1.7 nm), forming a DBQW structure. The DBQW structure was then surrounded by two 500 nm thick low-doped InGaAlAs spacer layers, which act as light absorption regions. The use of low-doped spacer layers can reduce the capacitance of the device to improve the frequency response. In addition, reducing the doping of the collector layers can enhance the electric field, which increases the velocity of photogenerated charge carriers on the collector side, resulting in shorter transit times and higher photodetection throughput. This InP/InGaAlAs system allows the realization of light detectors that cover the optical windows of 1300 nm and 1550 nm. This structure is then embedded between two 300 nm thick n-type highly doped InAlAs layers, followed by layers of highly doped InGaAs to form the contact. The fabricated size of the RTD-PD device is 10×10 μm^2 with an optical window of 36 μm^2, which provides direct optical access. A photograph of the device under test is shown in Fig. 13(a). Accordingly, the schematic structure of the circuit is presented in Fig. 13(b) [40]. Fig. 14 shows the current-voltage characteristic of the RTD-PD in the operating state of (a) electrical modulation and (b) optical modulation [40].

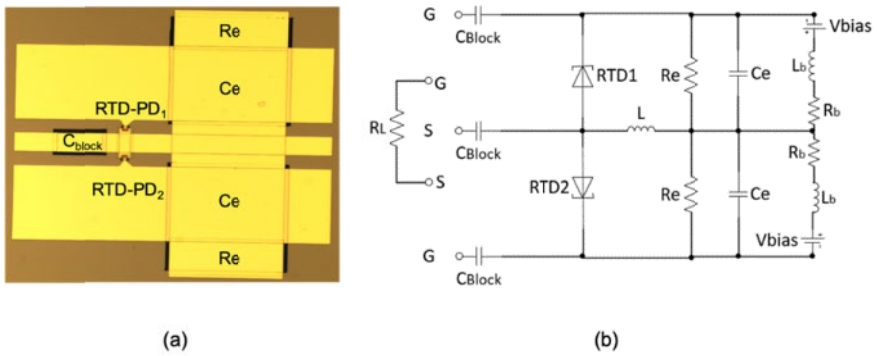

Figure 13 – (a) Photograph of a dual RTD-PD generator and (b) schematic structure of the generator [40]

An electronic RTD generator with the same circuit as in [40] was also demonstrated for wireless transmission in the 300 GHz frequency range with data rates up to 7 Gbit/s.

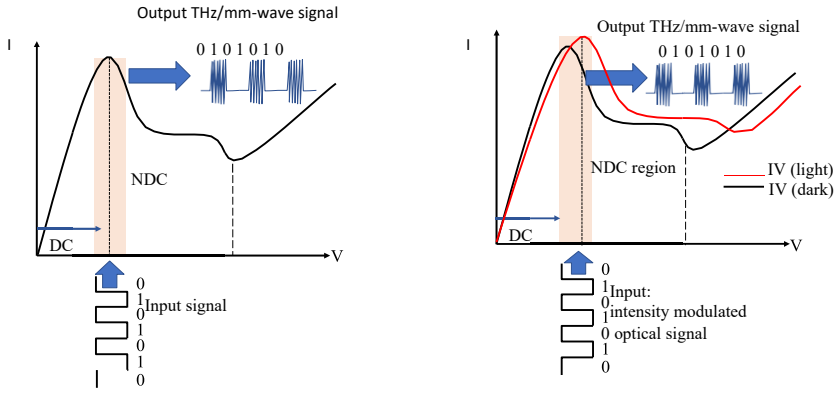

a) b)

Figure 14 – Current-voltage characteristic of RTD-PD in the operating state of (a) electrical modulation and (b) optical modulation [40]

1.4. Magnetic field sensors

Microelectromechanical systems (MEMS) technology includes products such as automotive airbag systems, display systems, and inkjet cartridges. It not only reduces the size of the device to the order of micrometers, but also integrates mechanical and electronic components on a single chip. This technology allows the design of portable devices such as gyroscopes, accelerometers, micromirrors, and pressure sensors [41]. For example, new cell phones include multiple MEMS devices such as gyroscopes, accelerometers, and magnetic field sensors for their global positioning system (GPS), and MEMS technology is expected to be a key driver of innovation in the mobile phone industry. Magnetic field sensors have great potential for numerous applications such as magnetic storage, automotive sensors, navigation systems, non-destructive material testing, security systems, structural stability, medical sensors, and military instruments [42]. Among the different types of magnetic field sensors, the superconducting quantum interference device (SQUID) is the most sensitive sensor, achieving a magnetic field resolution (minimum detectable magnetic field) of the order of a few fT [42] , and its operation is based on two effects: flux quantization and the Josephson effect (observed only in the presence of superconductivity). The device is mainly used in neuromagnetism (with signal levels of pT or lower), magnetic resonance, and geology [43]. On the other hand, magnetic sensors that use the Hall effect as the

conversion principle are usually fabricated using standard complementary metal-oxide semiconductor (CMOS) technology. Hall effect sensors are low cost and are used to measure linear position, angular position, velocity, and rotational speed. They are generally applicable for a sensitivity range of 1 to 100 mT and have a power consumption of 100 to 200 mW, a displacement of a few mT, and a matrix size of less than one millimeter. These sensors can measure both constant and alternating magnetic fields: the upper frequency limit is about 1 MHz and they work well in the temperature range from −100 to +100 °C [42]. However, silicon-based magnetic sensors may have intrinsic limitations in their sensitivity and resolution, which may limit future performance gains [43]. In addition, they require temperature compensation circuits, which may include a temperature sensor and operational amplifiers (OPs).

Search coil sensors detect only time-varying magnetic fields based on Faraday's law of induction. They can typically measure magnetic fields above 20 fT [43] and use a high-permeability ferromagnetic core inside the coil to increase their sensitivity. Typical coil dimensions are 0.05 to 1.3 m and power consumption is 1 to 10 mW. These sensors have a useful frequency range of 1 Hz to 1 MHz and are found on roads for traffic control [43]. The miniaturization of these sensors reduces their sensitivity, and they cannot detect static magnetic fields.

Ferrosonde sensors measure static or low-frequency magnetic fields and are sensitive to both field direction and field magnitude from 10-2 to 10 7 nT with a resolution of 100 pT [44]. Ferrosondes are the most widely used sensors for compass navigation systems, but they are also used for submarine detection, geophysical exploration, airborne magnetic field mapping, and electric current measurement. However, these sensors have a complex magnetic core and coil design, as well as high mass and power consumption. Any reduction in their mass and power reduces both their sensitivity and stability [44]. The frequency response of the sensor is limited by the excitation field and the response time of the ferromagnetic material. They can operate at frequencies up to 100 kHz, have dimensions of the order of a few millimeters, and consume power of about 100 mW. To miniaturize ferroprobe sensors, two problems must be solved: coil miniaturization and magnetic core integration.

Anisotropic magnetoresistive (AMR) sensors can achieve a sensitivity range of 10-1 to 107 nT [118], a typical resolution of 10 nT, and a size of a few millimeters [45]. These sensors are based on the anisotropic magnetoresistive effect that occurs in ferromagnetic transition metals, in which their electrical resistance depends on the angle between the electric current and the direction of magnetization. Therefore, an external magnetic field affects the direction of magnetization, causing a change in electrical resistance. AMR sensors have low sensitivity to mechanical loads and consume power of a few milliwatts [45]. Their applications include traffic counting, ground field sensing, electronic compasses, navigation systems, and wheel speed sensors for anti-lock braking systems (ABS). These sensors saturate at low magnetic fields (around a few mT) and require a complex reset procedure; furthermore, their sensitivity deteriorates when the power consumption decreases.

Giant magnetoresistive (GMR) sensors exhibit a large shift in electrical resistance when their thin (a few nanometers) layers of ferromagnetic and nonmagnetic materials are exposed to a magnetic field. Typically, they detect magnetic fields of 10 to 10 8 nT [46] and have a matrix size close to 1 mm. GMR sensors operate at temperatures above +225 °C. These sensors have found many applications, including magnetic read heads, vehicle detection and vehicle speed monitoring, pneumatic cylinder position sensors, crankshaft position sensors, current sensing, and silent locking mechanisms [46].

Fiber-optic sensors use the magnetostrictive effect to measure magnetic fields, whereby the dimensions of a magnetostrictive material change when placed in an external magnetic field [45]. This material is attached to a piece of optical fiber, which is used as the leg of a Mach-Zehnder interferometer, which measures the strain in the fiber under the action of a magnetic field. These sensors have a sensitivity range of 10-2 to 106 nT and are immune to electromagnetic interference (EMI) [46]. The challenge with this sensor is to identify and incorporate highly magnetostrictive materials into the fiber by appropriate bonding or coating, and the sensor is also sensitive to changes in temperature and pressure.

Recently, MEMS technology has been seriously considered as a candidate for sensor development due to its advantages such as small size, low weight, low power

consumption, low cost, high functionality, better sensitivity and resolution. This technology can integrate mechanical and electronic components on a common substrate, achieving the realization of complete systems on a chip. Therefore, some research groups have developed new resonant magnetic field sensors based on MEMS technology, which show important advantages in terms of their performance [47]. These sensors use resonant structures that use the Lorentz force principle to detect magnetic fields (Fig. 15). Typically, they measure the displacement of resonant structures exposed to external magnetic fields using capacitive, piezoresistive and optical measurement methods.

In [47], an ideal graphene-based magnetically tunable absorber in the terahertz (THz) region is proposed. The performance is analyzed using the 4×4 transfer matrix method, demonstrating that the ideal absorption frequency of the proposed absorber for left-handed circularly polarized (LCP) waves can be dynamically tuned by changing the external static magnetic bias field in three frequency ranges (0.95–2.2 THz, 4.15–5.4 THz, and 7.3–8.55 THz).

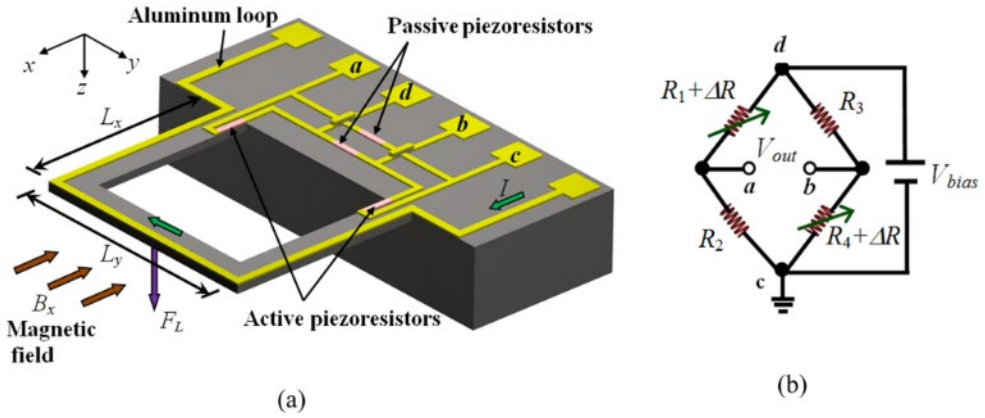

Figure 15 – (a) Schematic view of a resonant magnetic field sensor based on two U-shaped microbeams without clamps and (b) an associated Wheatstone bridge [47]

In addition, the proposed absorber can withstand a wide range of LCP wave incidence angles. Graphene is a two-dimensional honeycomb material with a single layer of carbon atoms [47]. It has been widely studied due to its unique electrical, mechanical, thermal and optical properties. In terms of electrical properties, the surface

conductivity can be tuned, and then graphene can be used in tunable devices such as modulators, filters and absorbers (Fig. 16).

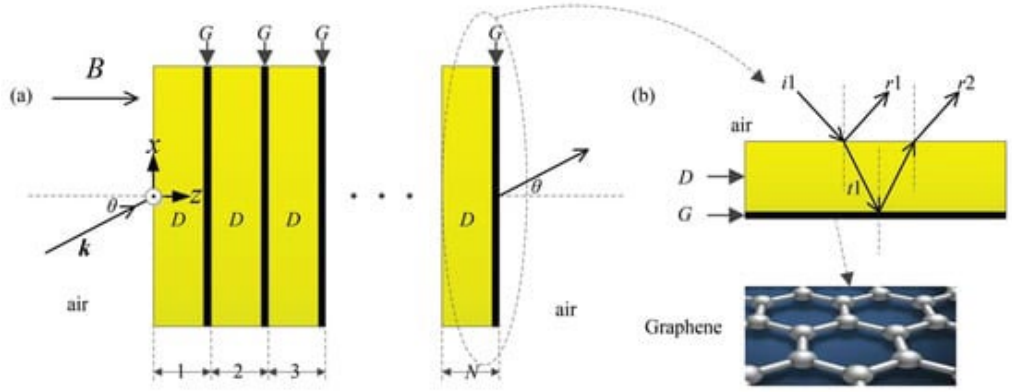

Figure 16 – Schematic of a graphene absorber model for the THz range

In particular, frequency-tunable absorbers have been widely studied from GHz to the infrared frequency range due to their extensive applications in sensors and detectors [48]. In the THz frequency range (i.e., 0.1–10 THz [48]), graphene supports strong surface plasmon polaritons and has strong photon localization, which greatly enhances the interaction between THz waves and graphene and effectively improves absorption [48].

In recent decades, magnetic field sensors based on magnetoelectric (ME) effects in composite heterostructures containing ferromagnetic (FM) and piezoelectric (PE) layers have been actively developed and investigated. ME sensors have high sensitivity and a large dynamic range, allow the detection of both constant and alternating magnetic fields, operate at room temperature, and have a simple design. In bulk composite heterostructures with sufficiently thick layers, ME effects arise due to the combination of magnetostriction of the FM layer and piezoelectricity in the PE layer due to the mechanical coupling of the layers [48]. When an alternating magnetic field is applied to the heterostructure, the FM layer deforms due to magnetostriction, this deformation is transmitted to the PE layer, and it generates an alternating electric voltage (direct ME effect) (Fig. 17). When the structure is excited by an alternating electric field, the PE layer deforms due to the inverse piezoelectric effect, the deformation is transmitted to the FM layer, which leads to a change in its magnetization

(inverse ME effect). In magnetic field sensors, the direct ME effect is mainly used .

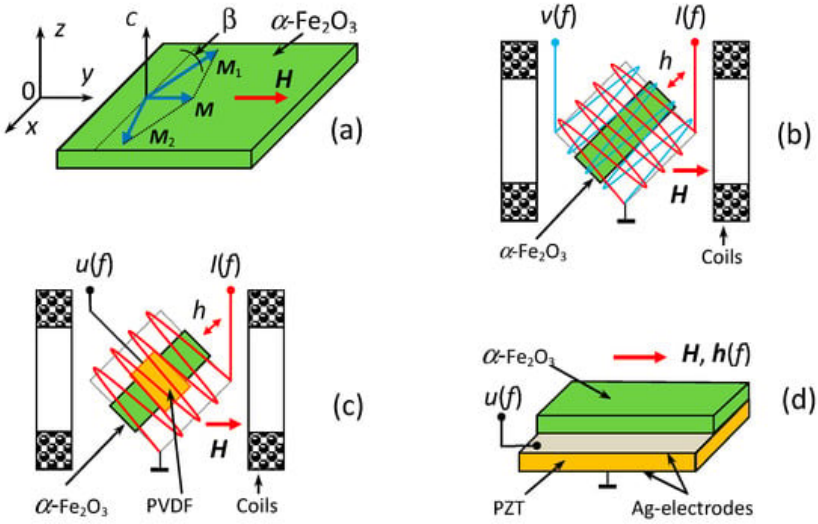

Figure 17 – (a) Schematic view of a magnetically sensitive composite heterostructure; (b) scheme of excitation and recording of magnetization oscillations in a hematite plate; (c) scheme of observation of the ME effect in a hematite-PVDF heterostructure; (d) schematic view of a hematite-PZT heterostructure

1.5. Pressure sensors

Microelectromechanical systems (MEMS) pressure sensors are widely used in consumer electronics, automotive systems, environmental monitoring, medical diagnostics, etc. [49]. According to the sensing principle, MEMS pressure sensors can be divided into three types, including piezoresistive pressure sensors, capacitive pressure sensors, and resonant pressure sensors. Compared with other pressure sensors, capacitive pressure sensor exhibits some significant advantages, such as high sensitivity, low power, low noise, and low temperature drift coefficients [49]. Various types of capacitive pressure sensors have been described in [50], but these designs do not contain any signal processing circuits, which leads to an increase in parasitic capacitance and a decrease in sensor performance.

Radio frequency identification (RFID), as a wireless automatic identification technology, is widely used in traffic management, logistics, transportation, medical

management, food production, etc. [50]. Passive RFID tag offers a number of advantages such as battery-free operation, wireless communication, high flexibility, low cost and fast deployment, which all lead to its wide applications in commercial use [51]. Passive RFID tag collects the radiation energy from the RFID reader as a power source. Therefore, the dissipation power of the passive RFID tag, which determines the maximum reading distance of the RFID reader, is crucial for the development of passive RFID tags. Recently, with the rapid development of the Internet of Things and sensor technology, research on adding sensor functions to RFID devices has become quite popular in consideration [51]. This smart RFID sensitive tag not only expands the application fields of RFID, but also helps reduce the manufacturing cost of information and measurement systems.

The operating frequency plays a very important role in RFID systems. In general, the operating frequency determines the data transmission rate between the transducer and the reader. A lower operating frequency usually means a lower data transmission rate. In addition to the data transmission rate, the operating frequency also determines the size of the tag. The operating frequency of RFID is mainly divided into three categories, namely: low frequency (LF—125 kHz), high frequency (HF—13.56 MHz), and ultra-high frequency (UHF—900 MHz) [143]. UHF—900 MHz RFID systems are the best solution for next-generation automatic identification applications because they have high transmission bandwidth and long-distance communication.

In [52], a block diagram of a passive wireless pressure sensor of a tag is proposed (Fig. 18). These blocks, except for the antenna, are integrated into a single-chip processor. The tag antenna, which is matched with the tag chip through a matching network, receives an electromagnetic wave from the RFID reader. The rectifier converts the received radio frequency (RF) signal into a stable supply voltage for the rest of the circuit. A voltage regulator is not included in the converter, since the capacitive sensor interface is insensitive to changes in the supply voltage value. When the rectifier output signal is set, the Power-On-Reset (POR) block generates a reset signal for the sensor interface. There is no receiver block in the tag, which means that the tag will work without any addressing as long as sufficient voltage is generated from

the incoming electromagnetic wave.

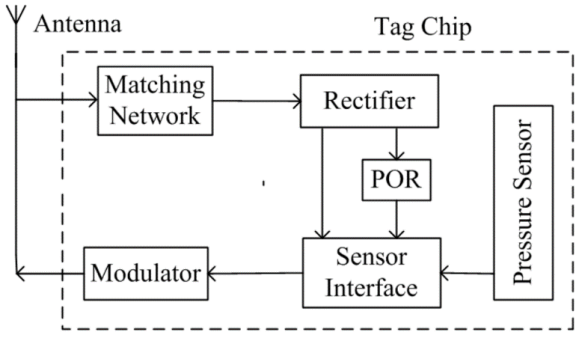

Figure 18 – Block diagram of the proposed passive wireless pressure sensor

The tag chip modulator uses a backscatter scheme. Backscatter is a low-power modulation scheme in which the RFID tag acts as a reflector that reflects the incident radio frequency wave back to the RFID reader. Backscatter can be amplitude shift keying (ASK) or phase shift keying (PSK). ASK backscatter is much simpler and more efficient than PSK backscatter [52], so the ASK backscatter scheme is used in this solution. In ASK backscatter modulation (shown in Fig. 19), when the switch (SW) is closed or open, the impedance of the chip changes between perfect matching (R in = R ant) and perfect mismatch (R in = 0) through a matching network, where R in is the input impedance of the chip and R ant is the antenna impedance.

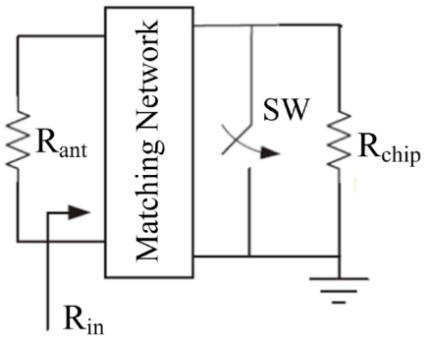

Figure 19 – ASK backscatter modulation

Capacitive pressure sensors [53] measure the capacitance between two electrodes with a variable distance due to a movable membrane. The basic structure of a capacitor consists of a set of parallel plates or electrodes with an area A separated by a distance d. The proposed pressure sensor [53] consists of three parts: the top electrode, the dielectric layer, and the bottom electrode. The dielectric layer consists of silicon oxide

and an air gap. The sensor fabrication process is shown in Fig. 20.

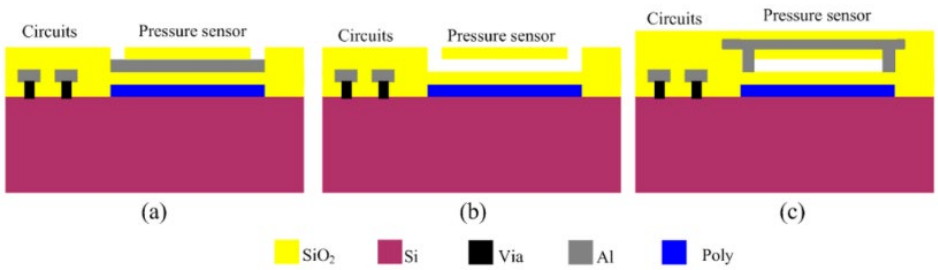

Figure 20 – Sensor manufacturing process; (a) after completion of the CMOS process; (b) etching of sacrificial sites; (c) sealing of the etching holes

A capacitive pressure sensor acts as a capacitor when it is connected to a sensor interface. There are several popular methods for performing the capacitance-to-digital conversion function. A general conversion starts with a capacitance-to-voltage converter followed by a voltage-to-digital converter [52, 53]. This technique can achieve high speed and high resolution. However, due to the use of an operational amplifier in switched capacitor amplifiers (SCAs), this technique introduces too much power dissipation, which is not suitable for passive designs.

In [54], a fully digital sensor interface (Fig. 21) is proposed, which is based on the theory of phase-locked frequency, which can achieve direct conversion of capacitance into digital signal. It consists of three blocks, including a sensor-controlled oscillator (SCO), a digitally controlled oscillator (DCO), and a phase detector (PD). Both the SCO and the DCO are implemented as three-stage ring oscillators based on an inverter. The sensor capacitor (C_{sens}) acts as a variable load on one stage of the SCO, thus generating a sensor-controlled frequency (f_{sens}). The DCO is controlled by the output signal PD (b_{out}), which is a representation of the phase difference between the SCO and the DCO. The variable capacitive load on one stage of the DCO consists of two capacitors Co and Cm. The capacitor C_o, designed to be equal to the quiescent value C_{sens}, is always connected to the DCO, but the capacitor Cm, designed to be slightly larger than the maximum variation of C_{sens}, is switched in or out of the DCO depending on the response from the PD. The PD simply consists of a single-bit d-flip-flop. The corresponding signals of this sensor interface for a constant sensor value are shown in Fig. 21,b. When the entire feedback loop is blocked, the average digital frequency (f_{dig})

will correspond to the sensor frequency (f_{sens}). Thus, the oversampled output (b_{out}) represents the digital value of the sensor capacitance.

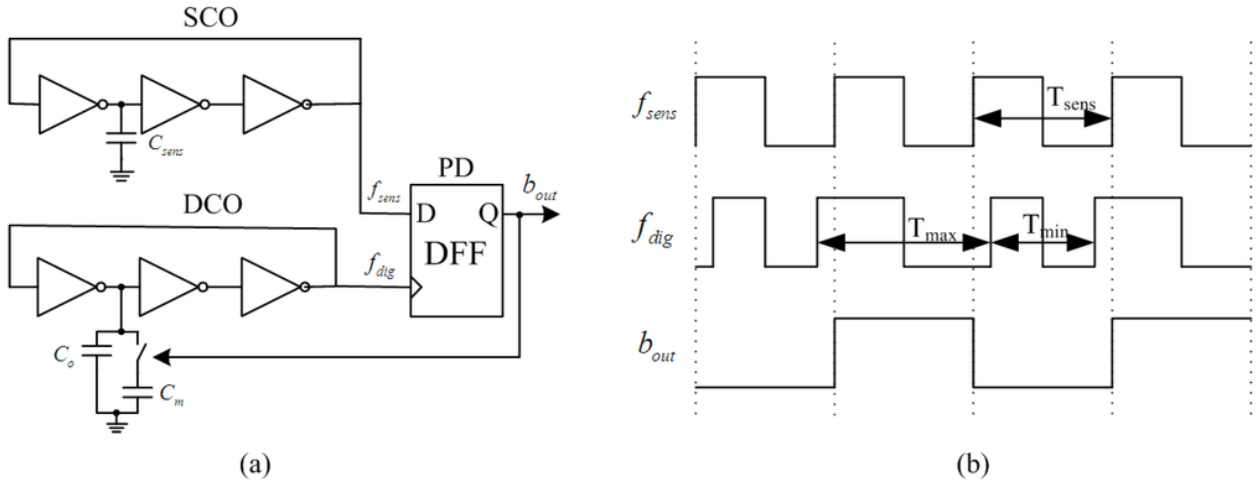

Figure 21 – Proposed fully digital capacitive sensor interface; (a) architecture; (b) corresponding waveforms for constant sensor value

Compared to the previous design, uses current-free ring oscillators to develop SCO and DCO. As shown in Fig. 22, M 1 – M 6 form a 3-stage inverter-based ring oscillator whose current is limited by the current mirror M 7 – M 12. Although the additional transistors M 7 – M 12 require a higher supply voltage, the current flowing through the inverters can be limited to a much lower value, resulting in lower power dissipation and higher temperature stability.

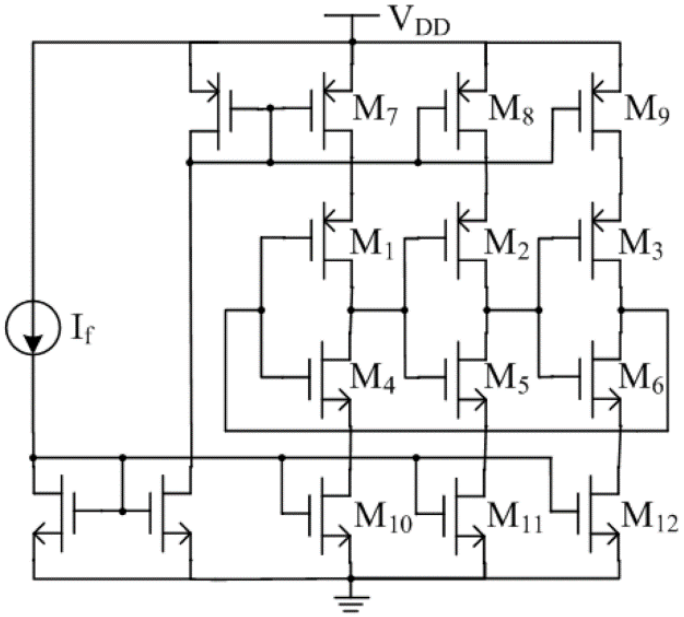

Figure 22 – Ring generator without current

Pressure measurement in high-temperature environments is of great importance in the aerospace, mining and metallurgy, and military industries [55]. During the operation of aerospace vehicles, the surface, engine, and gas turbine are usually accompanied by high temperature, high pressure, and other harsh environments. Therefore, it is necessary to accurately obtain the pressure parameter in real time to provide prerequisites and guarantees for the selection of surface material, structural design, and protective measures of aerospace vehicles. For example, when a hypersonic vehicle moves at high speed, the friction between the surface structure and the atmosphere releases a lot of heat. Accurate determination of the mechanical and thermal parameters of the surface is especially important for the design and protection of the surface structure.

In [55], a pressure sensor with integrated waveguide (SIW) on a passive substrate based on CSRR is proposed, which realizes the application of sensors in a high-temperature environment in the microwave frequency range using the principle of electromagnetic coupling. A small sealing cavity prepared by a three-dimensional integrated HTCC manufacturing process is placed under the CSRR. When the sealing cavity is deformed under pressure, the electromagnetic field near the CSRR resonator is disturbed, which leads to a shift in the resonant frequency. A schematic image of the CSRR pressure is presented in Fig. 23. The sensor consists of a SIW microwave cavity, a metal radiation spot with a CSRR structure, and a HTCC substrate with a sealed cavity. The HTCC substrate with a sealed cavity is manufactured by a three-dimensional integrated HTCC manufacturing process using 99% green HTCC ribbons. The SIW structure, consisting of parallel metal surfaces and metallized holes embedded in the substrate, has the advantages of high Q-factor, low environmental impact, and low insertion loss. The CSRR structure is embedded in a metal pad directly above the sealed cavity, using a metal line to transmit the signal and serving as the first high-reflectivity reflector.

The temperature and pressure applied to the pressure sensor can be precisely controlled by a high-temperature test platform. The pressure sensor needs to be measured in the pressure range of 10-300 kPa with an interval of 50 kPa at different

temperatures of 25-500 °C. At each temperature and pressure, the network analyzer outputs a corresponding frequency curve, and its negative peak value is the resonant frequency point of the sensor in this environment. Fig. 24 shows the measurement results of the sensor in the pressure range of 10-300 kPa at 25 °C.

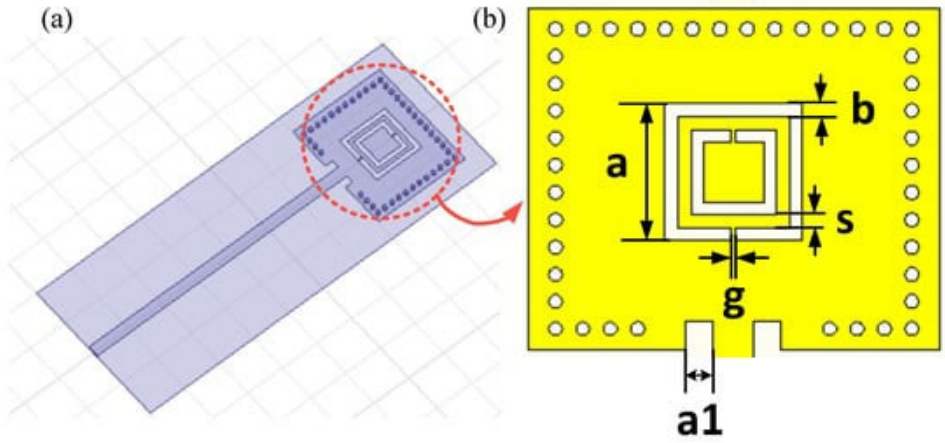

Figure 23 – CSRR sensor. (a) Simulation model in HFSS; (b) physical and geometric parameters of the built-in CSRR pressure sensor [56]

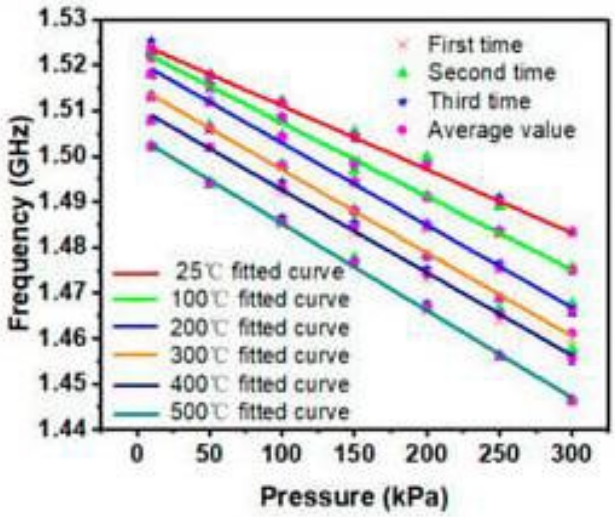

Figure 24 – Resonance frequency curves within the pressure range of 10–300 kPa at different temperatures [56]

The resonant frequency of the sensor decreases from 1.523 to 1.483 GHz when the pressure increases from 10 to 300 kPa at 25 °C. The pressure sensitivity of the sensor is 139.77 kHz/kPa at 25 °C. The pressure sensitivity of the sensor increases with increasing temperature. At 500 °C, the pressure sensitivity of the sensor is 191.97

kHz/kPa. This is because the increase in temperature softens the HTCC substrate, increases the cavity deformation distance under the same pressure, and increases the shift of the sensor resonant frequency, which leads to an increase in the pressure sensitivity of the sensor [56].

Wireless sensors with zero power consumption (i.e. passive or without built-in battery) and chip less (i.e. without electronic or integrated circuit) sensors are a very convenient solution for measuring any physical or chemical quantity, since their service life is unlimited, and remote monitoring of any physical and chemical quantities in harsh environments is possible. The geometry and topology of a passive microwave pressure sensor are presented in Fig. 25. As can be seen, the sensitive device consists of a thin flexible silicon membrane placed in the upper part of a circular cavity, inside which the resonator operates.

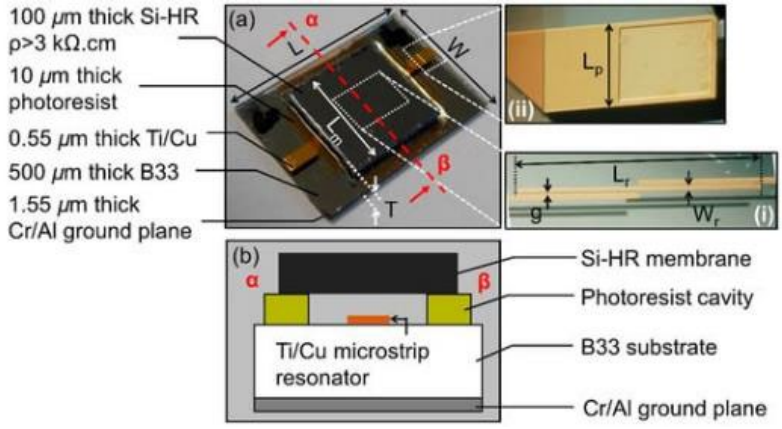

Figure 25 – Photographs of the microwave (24 GHz) sensor after bonding with its high resistivity (Si-HR) membrane

The resonator is a microstrip half-wave microwave resonator (24 GHz) designed to measure overpressures up to 2.1 bar (see Fig. 25). When a pressure gradient is applied between the inner and outer parts of the cavity, it causes both mechanical and electromagnetic effects on the passive sensor. This pressure gradient leads to deformation of the membrane and, as a result, causes a change in the gap between the membrane and the flat resonator. The resonant frequency of the resonator changes accordingly. At atmospheric pressure, f res and S 11 at fc = 23.8 GHz fluctuated at

approximately 23.65 GHz and -20.87 dB, respectively, during the experiment with oscillations of ±31 MHz and ±0.47 dB (i.e., an error of ±0.13% on f res and ±2.3% on the frequency of the S11 parameter). Taking into account the measurement errors at the calibration stage, the overall measurement accuracy of the resonant frequency and input reflection coefficient S 11 was ±44 MHz (±0.19%) and ±0.52 dB (±2.5%), respectively (Fig. 26).

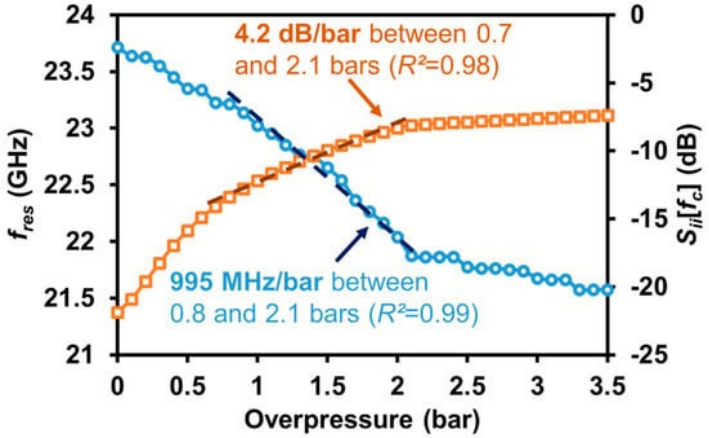

Figure 26 – Change in the resonant frequency f res and the input reflection coefficient S 11 from the change in pressure (b)

Resonant tunnel diodes (RTDs) and high electron mobility transistor (HEMT) based on GaAs, as a piezoresistive sensing element, demonstrate extremely high sensitivity in GaAs-based MEMS sensors [57].

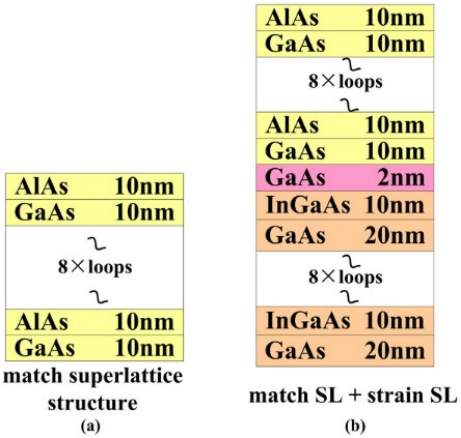

Figure 27 – Two different strain-sensitive RTD structures [57]

Due to their high electron mobility, low power consumption and photovoltaic characteristics, resonant tunneling diode (RTD) and high electron mobility transistor

(HEMT) are widely used as electronic devices and photovoltaic devices. RTD and HEMT show high piezoresistive coefficient, they can be used as sensitive elements of MEMS sensors [57]. From the experimental results, it has already been demonstrated that the sensitivity of MEMS using HEMT is two to three orders of magnitude higher than that using Si piezoresistive elements [57], and that of those using RTD is one to two orders of magnitude higher. In [57], two different solutions were used: AlAs/GaAs superlattice and InGaAs/GaAs strain superlattice (as shown in Fig. 27).

1.6. Humidity sensors

In addition to everyday applications such as air conditioners and humidifiers, humidity sensors are widely used in industrial process control, medicine, food processing, agriculture, and meteorological monitoring [58]. In industry, many manufacturing processes such as semiconductor manufacturing and chemical gas purification rely on precisely controlled humidity levels. In medical science, it is necessary to control the humidity of the environment during operations and pharmaceutical processing. In agriculture, humidity sensors are used for greenhouse conditioning, crop protection (dew prevention), soil moisture monitoring, and grain storage. In addition, in meteorological monitoring, weather bureaus and marine monitoring programs rely on accurate humidity measurements. For modern agriculture and weather stations, accurate and rapid humidity measurements are becoming increasingly important. Compared with existing infrared humidity sensors, electronic humidity sensors are cheaper, lighter, and smaller, making them more suitable for sensor networks to power weather models. However, high-precision sensors with fast response times are important for many applications. Therefore, electronic sensors need to become faster and more accurate.

Electronic humidity sensors can be divided into resistive and capacitive [59]. Resistive humidity sensors generally have a higher gain and are usually cheaper to manufacture than capacitive humidity sensors. However, these sensors do not respond well when operating at low relative humidity (approximately 10% RH) because they

exhibit very low conductivity in low relative humidity environments, making it difficult to measure the output signal response [59]. In contrast, capacitive humidity sensors have better linearity, accuracy, and higher thermal stability than resistive humidity sensors [59]. A capacitive humidity sensor responds to humidity changes by changes in the relative permittivity of a sensing layer, such as a polymer film, after water vapor is absorbed. Thus, capacitance changes can be directly detected to monitor humidity changes. Unlike a resistive humidity sensor, capacitive humidity sensors respond linearly to humidity, which simplifies reading the sensor.

Various materials can be used as humidity sensing materials, such as electrolytes, ceramics, porous inorganic materials, and polymers. In particular, polymers have been used as sensing materials for capacitive humidity sensors due to their good dielectric properties arising from their microporous structure and measurable changes in physical properties due to water absorption.

Capacitive humidity sensors have two basic structures: parallel plate capacitance (PP) (Fig. 28,a) and comb electrode capacitance (IDE) (27,b) [60].

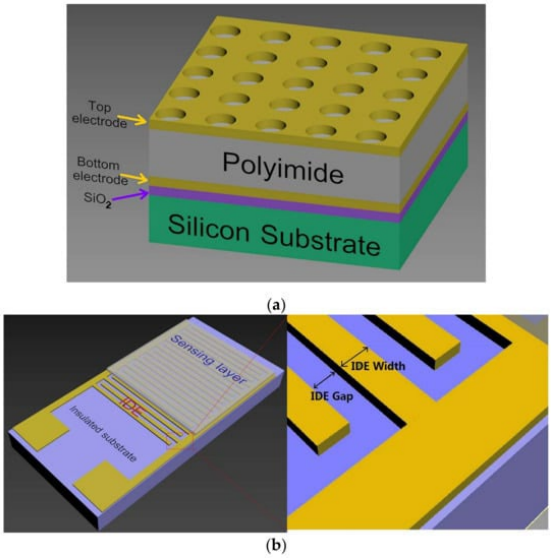

Figure 28 – Structural diagram of sensors with parallel plates (PP) and comb electrodes (IDE). PP sensors consisting of a solid substrate, two layers of parallel plate electrode and a sensitive material between them (a), IDE sensors consisting of an inert IDE substrate and a layer of sensitive material on top of the IDE (b) [60]

In [61], the design of the capacitive measuring transducer of the device is proposed, which is described below (Fig. 29). As we can see, both of its sensors consist of a system of flat plates (1), where two pairs of flat plates belong to measuring capacitors C1 and C4, and the remaining flat plates form another pair of measuring capacitors C2 and C3. All flat plates of the same length l are assembled inside two fluoroplastic rings (2) at an equal gap, denoted as Z. The measuring channel should be filled with a probe of liquid fuel under humidity control, and the reference channel with the same substance, but previously dehydrated. Using the method described above, it is necessary to measure the values of the electrical capacitances C1, C2, C3 and C4, and then calculate the differences C2 − C1 and C3 − C4. Once this is done, we can calculate the ratio of these differences (C3 − C4)/(C2 − C1), and this would be an informative parameter for further processing, directly related to the moisture content.

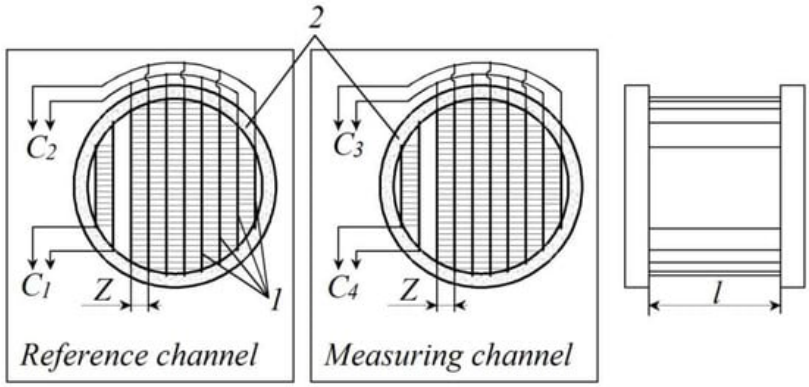

Figure 29 – Capacitive humidity measuring device (1 – flat electrode system, 2 – fluoroplastic rings) [61]

To implement this idea in practice, the authors [61] proposed a device for measuring humidity, which is shown in Fig. 30. As we can see, four capacitive sensors of the measuring converter are connected to the inputs of the corresponding monostable multivibrators MMV 1… MMV 4, designed to convert the values of the electric capacitance into the duration of rectangular pulses. The microcontroller controls the operation of the monostable multivibrators by generating rectangular pulses of a stable frequency at one of its output pins.

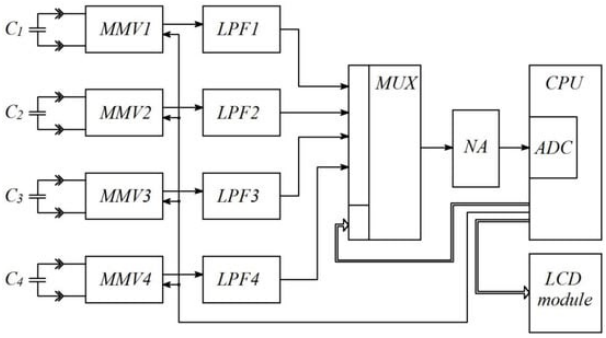

Figure 30 – Structural electrical diagram of the moisture meter (MMV1…MMV4 – monostable multivibrators, LPF1…LPF4 – low-pass filters, MUX – multiplexer, NA – normalizing amplifier, ADC – analog-to-digital converter) [61]

Each monostable multivibrator generates a sequence of rectangular pulses, the duration of which is directly proportional to the value of the electric capacitance connected to its input (diagrams in Fig. 31).

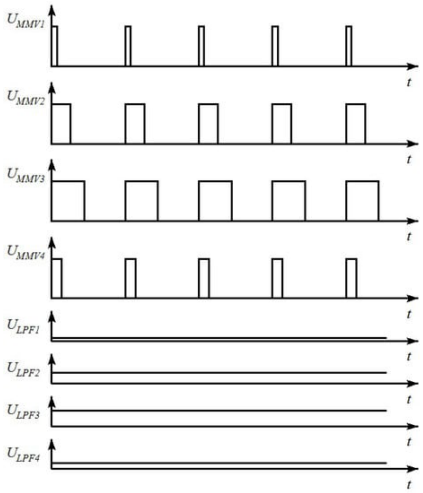

Figure 31 – Diagrams of the operation of the analog part of the moisture meter [61]

Low-pass filters convert the pulse duration into a DC voltage proportional to the amplitude of the pulse duration. In [62] presents a remote-powered microsystem for humidity measurement. The core of the active transponder consists of a humidity and frequency chip fabricated using standard complementary metal oxide semiconductor (CMOS) technology that contains both the humidity sensor and the readout circuit. The

sensor is fabricated using a polyimide passivation layer and a top metal layer. The same pair of inductively coupled coils with a carrier frequency of 13.56 MHz are used to transfer power and data to and from the chip. The humidity reading is transmitted by manipulating the load switching to an external circuit. The chip is fabricated using commercial 0.6-μm CMOS technology and occupies an area of 4.8 mm^2. The sensor capacitance has demonstrated good linearity over relative humidity (RH) levels from 15% to 85%. The normalized sensitivity is 0.073% per percent relative humidity at a temperature of 35°C. The total power consumption of such a humidity sensor is 1.39 mW. The device has two purposes; as a standalone wireless humidity sensor or for assessing the tightness of packages, for example, in biomedical implants.

In [63], a phase-frequency humidity sensor, its circuit design, measurement of the shift of the informative parameter due to the action of humidity, and manufacturing technology were investigated. The measurement circuit converts the electrical sensitivity of the transmission line conductor to the input phase as a measurement variable.

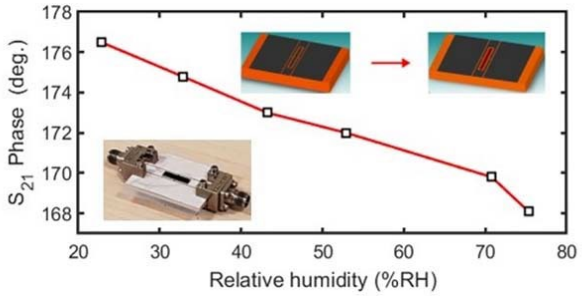

Figure 32 – Dependence of phase change on humidity change [63]

A coplanar waveguide (CPW) design was designed, printed, and tested under relative humidity (RH) conditions ranging from 22.8 to 75.3% RH. The authors [63] proposed the use of a composite material of polypyrrole and TEMPO oxidized cellulose nanofibers (TOCN/PPy) as a sensing element, which was integrated into the structure and investigated as a moisture-sensitive conductor at microwave frequencies (Fig. 32). The measured sensitivity was 0.154°/%RH at 5.870 GHz, while the insertion loss decreased by 1.26 dB.

1.7. Gas sensors

In the past few years, the Internet of Things (IoT) has played a significant role and improved the quality of life in various fields. In the world of digitalization, various objects are cooperating with the Internet of Things (IoT); these objects are also enhanced with sensing and data processing structures. Radio Frequency Identification (RFID) has been identified as a key technology contributing to the IoT. In the RF mode, many sensors are based on various devices from passive components to active components. These microwave sensors are characterized by an operating frequency or S-parameter, which is defined as the ratio of the output port voltage to the input port voltage when all other ports are terminated with matched loads. Due to their cost-effectiveness, reusability, and low power consumption, as well as multi-parameter measurement, microwave sensors have been used in various applications for decades. Microwave sensors exhibit analytical properties by varying their characteristics such as operating frequency, reflection coefficient, transmission coefficient, and phase.

Metal-oxide semiconductors (MOS) are advanced multifunctional materials that are considered prime candidates for use in resistive gas sensors due to their high sensitivity, chemical and temporal stability, wide and tunable band gap, simple fabrication technology, and cost-effectiveness [64]. One of the most widely used MOS in gas sensors is iron oxide, which is an inorganic compound with the chemical formula Fe_2O_3. It appears in two polymorphic forms, α and γ, of which α-Fe_2O_3 (hematite) is an inexpensive, common, environmentally friendly, and non-toxic material with a tunable band gap (~2.1 eV). The most stable form of iron oxide, hematite, exhibits excellent gas-sensing characteristics. Furthermore, the electrical, chemical, and gas-sensing properties of α-Fe_2O_3 can be significantly improved by functionalizing the material using bulk dopants (or solid solutions) and noble metal nanoparticles as surface enhancements [65]. In the last decade, ZnO-based nanostructures have become one of the most widely used metal oxides in the fabrication of nanostructured gas sensors due to their unique sensing behavior, high electron mobility (~400 cm 2 V-1 s-1), wide band gap (3.37 eV), and large excitation binding energy (60 meV). In

addition, nanocomposite structures based on multicomponent materials exhibit much better gas detection performance than the pure materials themselves [66].

The use of polymers as gas-sensitive materials has many advantages over other materials, as they can be used with different chemical structures and tunable surface functional properties. Let's consider the PANi sensor mechanism.PANi also reacts with gases through a redox reaction, but PANi has the characteristics of partial charge transfer. The direction of partial charge transfer is determined by the work function of the conducting polymer and the electronegativity of the gas vapor [66]. Partial charge transfer consists of electron transfer and proton transfer. When PANi is exposed to carbon monoxide (CO), electrons in the PANi film are removed, and the resistance of PANi decreases [66]. The specificity of PANi is that the doped state is controlled by the acid-base reaction. Therefore, PANi is widely used for the detection of acidic and basic gases.

The conducting polymer PANi has the advantages of environmental stability and ease of synthesis. In [67], the electrical dielectric and reflection loss of PANi synthesized with different ratios of $BaTiO_3$, which is a ferroelectric material with high resistivity, were analyzed and these samples were measured at microwave frequencies in the X-band (from 8.2 to 12.4 GHz). They found that the DC or AC conductivity, dipole relaxation and reflection loss increased with increasing PANi content. They also found that BaTiO3-PANi could be used as an absorber and the frequency coherence decreased with increasing thickness of BaTiO3-PANi.

In [67], the relative dielectric and relative permittivity of PANi synthesized with cobalt ferrite ($CoFe_2O_4$) were measured in the Ku band (12.4 to 18 GHz). The PANi:$CoFe_2O_4$ ratios were 2:1, 1:1, 1:2, and 1:3. They analyzed the electromagnetic shielding efficiency (SE), which is defined as the ratio of transmitted power to incident power. The SE of each sample was analyzed by dividing the SE due to absorption by the SE due to reflection. They found that the SE of PANi-$CoFe_2O_4$ was mainly due to absorption and the SE of PANi-$CoFe_2O_4$ increased with increasing $CoFe_2O_4$ content.

Let's consider the PEDOT sensing mechanism. PEDOT exhibits high stability and high conductivity in the oxidized state. However, to improve the characteristics of

PEDOT, PEDOT is usually combined with poly (styrene sulfonate) (PSS). The combination of two PEDOT cations with negatively charged PSS anions formed PEDOT:PSS. PEDOT:PSS is soluble in water and has improved conductivity and stabilization. PEDOT:PSS can be used as a sensing material for the detection of ethanol gas, alkane, and water vapor via redox reactions. PEDOT:PSS undergoes electron transfer and changes resistance depending on the specific gas. When PEDOT:PSS reacts with electron donors such as gaseous ethanol and alkane, the electrical conductivity of PEDOT:PSS increases. On the other hand, when PEDOT:PSS reacts with water vapor, which is an electron acceptor, the electrical conductivity of PEDOT:PSS is enhanced.

Consider radio frequency chemical gas sensors using conductive polymers. PANi is widely used for various gas sensors at radio frequencies. Shen et al. proposed a wireless passive gas sensor based on LC mutual coupling. The LC resonator based on interdigitated electrodes was designed to resonate at a frequency of 213.6 MHz. PANi was synthesized from CNTs, and the PANi/CNT composite was placed on a multi-pin electrode. The PANi/CNT-based gas sensor was fabricated as shown in Fig. 33. When the sensor was exposed to ammonia, the capacitance of the interdigitated electrode changed and a resonant frequency shift occurred. When the sensor was exposed to 100, 200, and 300 ppm of ammonia gas, the resonant frequency shifts were 4.352 MHz, 9.235 MHz, and 12.070 MHz, respectively, as shown in Fig. 32b. It was demonstrated that the sensitivity of the PANi/CNT-based sensor is approximately 40 kHz/ppm at a concentration of 300 ppm, and the change in the resonant frequency is large at low ammonia concentrations.

Surface acoustic wave (SAW) sensors are widely used for gas detection using PANi. SAW sensors are suitable for gas measurement due to their high sensitivity, fast and reliable response, potential for wireless sensing, small size, and low power consumption [68]. A shear horizontal surface acoustic wave (SH-SAW) sensor coated with a PANi film was proposed to detect the presence of ammonia [68]. The proposed SH-SAW sensor operated at 148 MHz. The sensor detected the concentration of gaseous ammonia from 20 ppm to 70 ppm by frequency shift. They also presented a

Rayleigh surface acoustic wave (RSAW) sensor with a copper-doped PANi-SnO_2 nanocomposite thin film to detect the presence of nitric oxide (NO) at room temperature.

The RSAW was operated at 98.47 MHz, and the sensor detected NO from 100 ppb to 350 ppb with frequency shift. Shi et al. also proposed a SAW-based gas sensor at 146 MHz. Palladium phthalocyanine (PdPc)-PANi was used as a sensing material for the detection of phosphorus-containing toxic gas. When the sensor was exposed to dimethyl methylphosphonate (DMMP), it demonstrated a sensitivity of 550 kHz/ppm.

In [69], a PANi/tungsten trioxide (WO_3) nanofiber composite SAW sensor was proposed for hydrogen (H_2) detection by frequency shifting at 107.2 MHz. The range of H_2 was from 0.06% to 1%. It was demonstrated that the sensor response was 7 kHz with 1% H_2. They also studied a PANi/In_2O_3 SAW sensor for H_2, carbon monoxide (CO) and nitrogen dioxide (NO_2) detection by frequency shifting [69]. The sensor response was 11 kHz, 2 kHz and 2.5 kHz up to 1% H2, 500 ppm CO and 2.12 ppm NO_2, respectively.

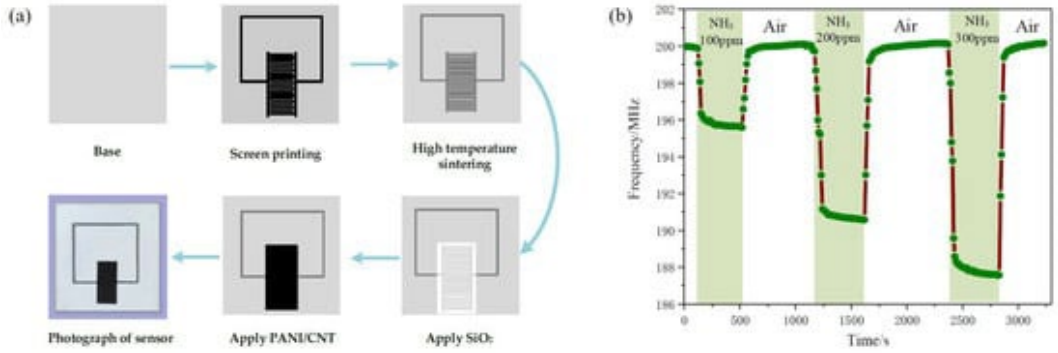

Figure 33 – Characterization of ammonia gas sensor based on PANi/CNT composite. Sensor fabrication process (a). Response curve and recovery time with different concentrations of ammonia gas (b)

In [70], a wireless radio frequency identification (RFID) sensor using carboxyl functionalized PPy nanoparticles (C-PPy) at 940 MHz was proposed. The C-PPy nanoparticles are used as a sensing material for ammonia gas detection and are deposited on the RFID sensor tag, as shown in Fig. 34a. When the sensor was exposed to ammonia in the range of 0.1 ppm to 25 ppm, the reflectance was as shown in Fig.

34b. The sensor demonstrated ultra-high sensitivity to ammonia, detecting concentrations as low as 0.1 ppm.

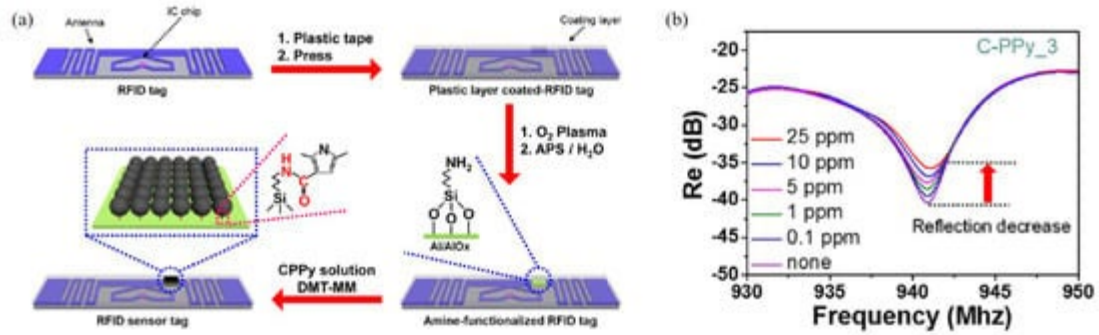

Figure 34 – Characterization of RFID-based ammonia gas sensor with C-PPy. (a) Schematic of RFID sensor tag with C-PPy nanoparticles in desired position. (b) Variation of reflectance of C-PPy-based RFID sensor tag [70]

In [71], a gas sensor based on SAW with nanofibers was presented. The operating frequency of the SAW sensor was 90.6 MHz, and gases were detected by frequency shift. As a result, the sensor response was 20 kHz to 1% H_2 and 4.5 kHz to 2.1 ppm NO_2. In [71], a nanoparticle-based SAW-based acetone gas sensor was proposed, as shown in Fig. 35. The SAW-based sensor was operated at 300 MHz, and the change in the operating frequency was monitored for acetone detection. The nanoscale structure of PPy provides a large surface area and provides high sensitivity and fast response time. The sensor response was linear with acetone concentration in the range of 5.5 ppm to 80 ppm. The resulting frequency shift was 10.9 kHz with 80 ppm acetone.

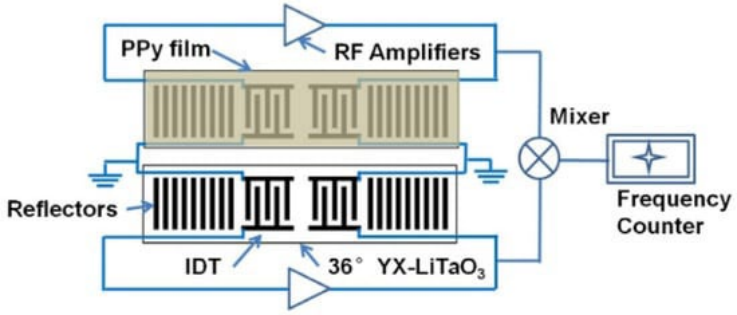

Figure 35 – Scheme of a gas sensor based on surfactants

A comb gas sensor based on a PEDOT:PSS resonator was proposed in [72]. The resonant frequency of the comb resonator was 3.584 GHz, and the sensor detected

gaseous ammonia in the range from 50 ppm to 2000 ppm in terms of frequency shift. In [72], an ethanol sensor based on a double-strip circular ring resonator (DSRR) loaded with PEDOT:PSS at 14.86 GHz was proposed. When the end of the microstrip line was connected to the input signal source, a magnetic field was induced to the DSRR, as shown in Fig. 36a. The transmittances of the ethanol sensor are shown in Fig. 36b. 100 ppm ethanol gas was detected by the resonant frequency and transmittance. According to the measurement results, when the sensor was exposed to 100 ppm ethanol, the oscillations of the resonant frequency and the transmission coefficient were 220 MHz and 0.79 dB, respectively. In [72], a PEDOT:PSS gas sensor to a hybrid coupler operating at 2.4 GHz was proposed, as shown in Fig. 37a. As shown in Fig. 37b, the PEDOT:PSS transmission line can be represented as a variable impedance Z11. When the ethanol gas molecules reacted with the PEDOT:PSS, Z11 was changed due to the adhesion of the ethanol gas molecules.

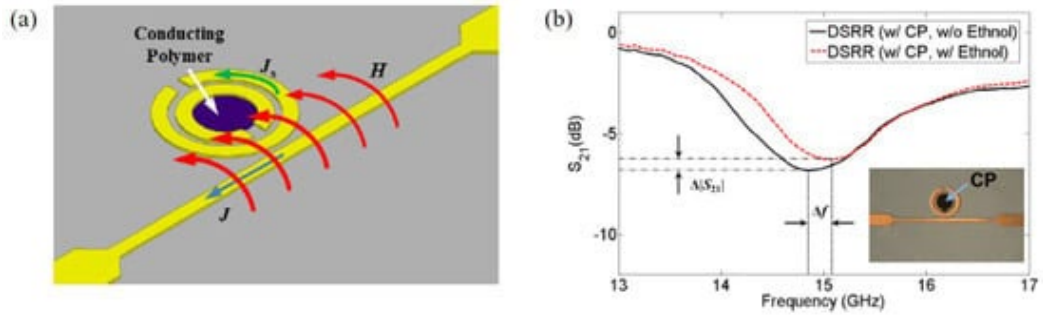

Figure 36 – Ethanol gas sensor with DSRR and PEDOT:PSS. (a) Mechanism of operation of DSRR for gas detection using conductive polymer. (b) Transmittances of the sensor with and without ethanol

Then the reflection was changed, and 100 ppm of ethanol gas could be detected by frequency and phase shift, as shown in Fig. 37c. Therefore, when the sensor was exposed to 100 ppm of ethanol gas, the frequency and phase fluctuations were 2.875 MHz and 9.09 degrees, respectively.

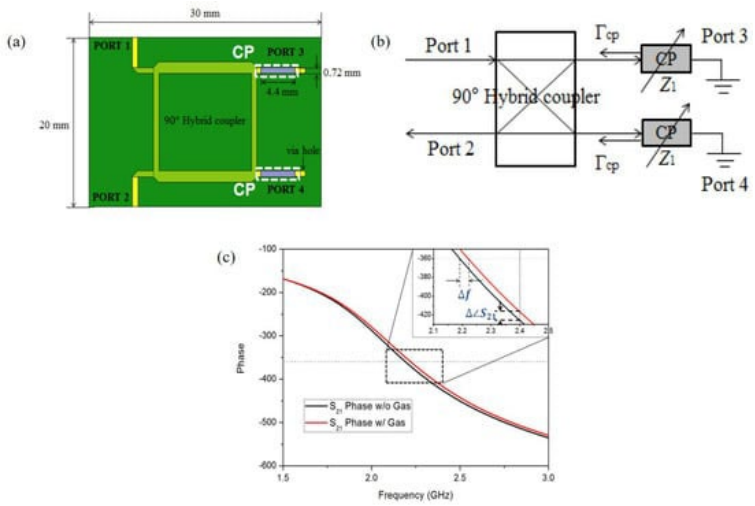

Figure 37 – Ethanol gas sensor with hybrid linker and PEDOT:PSS. (a) Schematic diagram of the sensor. (b) Equivalent circuit of the sensor. (c) Phase response of the sensor with and without ethanol [72]

Summary and conclusions

nalysis of publications devoted to theoretical and experimental research radio engineering devices for measuring physical quantities in wireless sensor networks control and management systems, shows that the creation of radio engineering devices for measuring physical quantities based on self-oscillating devices with parametric sensitive transducers for radio engineering and electronic communication systems is a promising scientific direction, because in this case high metrological and economic indicators of devices are realized and the transmission of controlled information over a distance and technological compatibility with microelectronic information processing devices are possible. Analysis of methods for measuring physical quantities at the current stage of development of science and technology has shown that measuring devices are at the initial stage of development and are based on the conversion of an analog signal from primary converters into a code signal based on an ADC and subsequent information signal processing schemes, which complicates information and measuring equipment.